AD-A253 314

(2)

Annual Technical Report to:

The Office of Naval Research and

The Strategic Defense Initiative Office of Innovative Science and Technology

for the Project:

"Advanced Transport Systems for Electron Beams in High-Brightness Accelerators and FELs"

(ONR Contract: N00014-91-J-1941)

DTIC
ELECTE
JUL 3 1 1992
S D
A

Submitted by:

R. M. Gilgenbach,
Principal Investigator

T. Kammash and M.L. Brake,
Co-Principal Investigators

Nuclear Engineering Department
University of Michigan
Ann Arbor, MI 48109-2104

This document has been approved for public release and sale; its distribution is unlimited.

July 1992

92-20529

92 7 2 043

REPORT DOCUMENTATION PAGE

Form Approved
OMB No. 0704-0188

Public reporting burden for this collection of information is estimated to average 1 hour per response, including the time for reviewing instructions, searching existing data sources, gathering and maintaining the data needed, and completing and reviewing the collection of information. Send comments regarding this burden estimate or any other aspect of this collection of information, including suggestions for reducing this burden, to Washington Headquarters Services, Directorate for information Operations and Reports, 1215 Jefferson Davis Highway, Suite 1204, Arlington, VA 22202-4302, and to the Office of Management and Budget, Paperwork Reduction Project (0704-0188), Washington, DC 20503.

1. AGENCY USE ONLY (Leave blank)	2. REPORT DATE	3. REPORT TYPE AND DATES COVERED
	July 24,1992	Annual:5/1/91 to 5/31/92

4. TITLE AND SUBTITLE
Advanced Transport Systems for Electron Beams in High Brightness Accelerators and FELS

5. FUNDING NUMBERS
ONR Contract
SFRC Number
N00014-91-J-1941

6. AUTHOR(S)
R. M. Gilgenbach, T. Kammash, M. L. Brake

7. PERFORMING ORGANIZATION NAME(S) AND ADDRESS(ES)
Nuclear Engineering Department
University of Michigan
Ann Arbor, MI 48109-2104

8. PERFORMING ORGANIZATION REPORT NUMBER

9. SPONSORING/MONITORING AGENCY NAME(S) AND ADDRESS(ES)
Strategic Defense Initiative
Innovative Science and Technology/
Office of Naval Research

10. SPONSORING/MONITORING AGENCY REPORT NUMBER

11. SUPPLEMENTARY NOTES

12a. DISTRIBUTION/AVAILABILITY STATEMENT
Approved for public release;
distribution is unlimited.

12b. DISTRIBUTION CODE

13. ABSTRACT *(Maximum 200 words)*

Research has concentrated on the excitation and stabilization of the beam-breakup (BBU) instability in high current, long-pulse electron beam transport through microwave cavity systems. Electron beams are generated by the Michigan Electron Long Beam Accelerator (MELBA) at parameters: 0.7 to 0.8 MV, $I_{injected}$ =40-400 A, and pulselength = 0.5 μs. Major accomplishments include:

1) Successful excitation of the beam-breakup (BBU) instability by microwave priming of the first cavity of a ten-RF cavity system,

2) Measurements of BBU growth as a function of priming frequency, confirming that the TM_{110} BBU mode was responsible for the growth,

3) Characterization of the BBU growth rate as a function of magnetic field and e-beam current,

4) The first experiments demonstrating that external-coupled-cavities reduce the growth rate for the BBU instability, and

5) Development of a theory for the beam breakup instability in quadrupole and solenoidal electron beam transport systems.

14. SUBJECT TERMS	15. NUMBER OF PAGES
Electron beams, accelerators, beam-breakup-instability	47
	16. PRICE CODE

17. SECURITY CLASSIFICATION OF REPORT	18. SECURITY CLASSIFICATION OF THIS PAGE	19. SECURITY CLASSIFICATION OF ABSTRACT	20. LIMITATION OF ABSTRACT
UNCLASSIFIED	UNCLASSIFIED	UNCLASSIFIED	Unlimited

NSN 7540-01-280-5500

Standard Form 298 (Rev 2-89)
Prescribed by ANSI Std 239-18
298-102

Table of Contents

Accesion For
NTIS CRA&I
DTIC TAB
Unannounced
Justification
By
Distribution /
Availability Codes
Dist | Avail and / or Special
A-1

DTIC QUALITY INSPECTED 8

1.0 Summary

Significant progress has been made on experimental studies of electron beam stability in accelerator transport systems during the past year. Research has concentrated on the excitation and stabilization of the beam-breakup (BBU) instability in high current, long-pulse electron beam transport through microwave cavity systems. Electron beams are generated by the Michigan Electron Long Beam Accelerator (MELBA) at parameters: 0.7 to 0.8 MV, $I_{injected}$ =40-400 A, and pulselength = 0.5 μs. Major accomplishments include:

1) Successful excitation of the beam-breakup (BBU) instability by microwave priming of the first cavity of a ten-RF cavity system,
2) Measurements of BBU growth as a function of priming frequency, confirming that the TM_{110} BBU mode was responsible for the growth (to be published in Applied Physics Letters on August 10, 1992)
3) Characterization of the BBU growth rate as a function of magnetic field and e-beam current,
4) The first experiments *demonstrating that external-coupled-cavities reduce the growth rate for the BBU instability,* and
5) Development of a theory for the beam breakup instability in quadrupole and solenoidal electron beam transport systems.

These accomplishments will be discussed in further detail in the following sections.

2.0 Experimental Configuration

The basic experimental configuration for the beam breakup instability priming experiments is depicted in Figure 1. The beam generator is the Michigan Electron Long Beam Accelerator, (MELBA), operating at parameters of V=0.8 MV, I_{diode}=1-15 kA, and pulselengths typically from 0.5-1 μs. The cathode consists of a cotton velvet-covered button on the end of the hemispherical cathode stalk. This cathode gives minimal diode closure and yields fairly flat current throughout the pulse. Large pulsed magnetic field coils surround the diode chamber and produce a magnetic field of about 0.8 kG. A graphite apertured anode plate is used to extract a beam of 2 cm diameter. The extracted electron beam current is measured by a Rogowski coil in the anode flange. The beam passes through a small-diameter tube with its own Rogowski coil before entering the first of 10 cavities. The RF cavities have a radius of 6.9 cm and a length of 2 cm. This gives a TM_{110} mode resonant frequency of 2.5 GHz, which matches the frequency of our priming source. The ten cavities are

separated by 3.8 cm diameter copper tubes which prevent electromagnetic crosstalk between cavities which would otherwise lead to the regenerative beam breakup instability. Inside each microwave cavity is a small coupling loop designed to detect the TM_{110} mode power. In the microwave priming experiments the first cavity coupling loop was driven by a kW level magnetron. The RF growth due to the beam breakup instability was measured by a comparison of the second cavity and tenth cavity powers. Signals from the two monitored cavities were transmited to the Faraday cage for detection on crystal detectors. The exiting electron beam current is measured by a Rogowski coil on the output tube after the last cavity and by a current collector grounded by a braided cable which passes through a Pearson coil.

The solenoidal focusing coil is wound directly on the stainless steel vacuum chamber. This magnetic field coil is energized by a large electrolytic capacitor bank. This solenoidal coil system is capable of up to 4 kG.

Different cavity Qs were used to perform two sets of experiments on beam breakup instability growth. In the case 1 set of experiments, the Qs were large, about 1,000 (see Table 1), with moderate frequency spread between the cavity resonance frequencies. In case 2 the Qs were lowered by placing microwave absorber rings in the cavities; the frequency spread was also lowered between the cavities down to about 0.1 %.

Table 1. Cavity Parameters for High-Q and Low-Q Cases

		Case 1		Case 2	
	Cavity #	TM_{110} freq. (GHz)	Q	TM_{110} freq. (GHz)	Q
(Driven)	1	2.5190	660	2.5070	230
(Probed)	2	2.5200	1090	2.5070	290
	3	2.5200	1420	2.5060	215
	4	2.5201	1800	2.5066	220
	5	2.5265	530	2.5071	280
	6	2.5270	680	2.5076	230
	7	2.5230	1160	2.5082	160
	8	2.5240	920	2.5082	185
	9	2.5248	680	2.5085	180
(Probed)	10	2.5250	1010	2.5086	170

Case 1 Average Frequency: 2.5230 GHz ± 0.3 %
Average Q: 1000 ± 310

Case 2 Average Frequency: 2.5075 GHz ± 0.1 %
Average Q 215 ± 45

3.0 Experimental Results

3.1 High-Q, Large Frequency Spread Between Cavities

The data taken with high Q (1000) and large frequency spread are shown as a function of current in Figure 2. It can be seen that for this case, the theoretical growth differed significantly from the experimental growth, especially at high currents. This is due to both the large frequency spread of the cavity resonance frequencies and to electron beam-induced detuning of the cavitiy resonance at high currents. The high Q of the case 1 system made it difficult to get sufficient overlap of the Q curves. Essentially the resonance frequency spread appeared to give the effect of stagger tuned cavities, which would give lower growth rate than expected.

3.2 Low-Q, Small Frequency Spread Between Cavities

The lower Q (215) case also had much less frequency spread between cavities (<0.01%), yielding much better overlap of the Q curves. This gave much improved agreement between theory and experiment and also made it possible to perform successful coupled-cavity BBU reduction experiments. Figure 3 shows excellent agreement of BBU experimental growth rates compared to theory. The scaling of the BBU growth was measured as a function of the microwave priming frequency, as shown in Figure 4. It can be seen that strong BBU growth is only observed when the priming frequency was set almost exactly (+0.05 GHz) equal to the TM_{110} resonance frequency. This proves that the measured microwave growth is due to the TM_{110} BBU mode. Figure 4 also compares the experimental BBU growth with both of the theoretical formalisms: continuum and discrete cavity. The discrete cavity theory agrees very well with the experimentally measured growth rate. Although the continuum theory agrees less well with the experiment, it should be stressed that a ten cavity system with cavity spacing comparable to the betatron wavelength is a stringent test of continuum theory.

The final part of the previous year's research was a test of the concept of BBU growth reduction by coupling external (dummy) cavities to the internal (e-beam) cavities. The experimental configuration for coupled-cavity BBU reduction experiments is given in Figure 5. As in the previous BBU experiments, the first cavity was primed and RF power was measured in the second and tenth cavities. However, the seven intermediate (beam) cavities (#3 through #9) were coupled to external (dummy) cavities by microwave coaxial cable. Typical experimental data are presented in Figure 6 (uncoupled case) and Figure 7 (coupled-cavity

case). These two consecutive shots show a factor of 4 reduction in the BBU RF power, (Fig. 6c compared to Fig. 7c).

A series of some 40 shots was run by alternating between three shots for each case, (coupled vs. uncoupled). These data are displayed in Figure 8. The average BBU growth for uncoupled cavities was 36 dB. For seven-pair of coupled cavities, the beam breakup instability growth was reduced to about 30 dB. Thus, we measured a 6 dB reduction in beam breakup growth by 7-coupled-cavity pairs. *These are the first experiments which have demonstrated a reduction of the beam breakup instability growth rate by external-coupled-cavities.* The scatter in the data is probably due to shot-to-shot fluctuations in the beam current, as shown in Figure 9. It should be noted that the amount of cavity coupling was not optimized in these experiments. Greater BBU reduction could have been achieved with higher beam-cavity-to-external-cavity coupling. This is a subject of ongoing study in the current year's research.

4.0 Theoretical Research

The theoretical research program has derived dispersion relations in order to calculate the growth rate, dominant wavelength, and group velocity of the beam-breakup instability. The dispersion relations have been found for a number of different cases:

1) Weak and strong focusing,
2) solenoidal, (2-dimensional theory) versus quadrupole, (1-dimensional theory) focusing systems,
3) various spacing of the accelerator cavities, and
4) periodically pulsed beams.

These investigations have shown that the BBU growth is minimized when the cavity spacing is an integral number of betatron wavelengths for solenoidal focusing or spacing by an integral number of half-betatron wavelengths for quadrupole focusing. These theoretical results are described in detail in an article published in Journal of Applied Physics (see Appendix).

Two interesting phenomena were examined in connection with the beam breakup instability: one dealing with the effects of the beam betatron frequency spread and the other having to do with the effects of the cavity frequency spread. In the first case, an appropriate dispersion equation was solved and the results can be summarized as follows: The fastest growing modes have about the same growth rates as without the spread, but are shifted to a much larger wavelength regime. For a mode which is initially stable, unlike the no-betatron frequency spread case, it can grow unstable with a substantial growth rate over a wide pressure range.

When cavity mode frequency spread is examined, a beam Bennett distribution was employed where it is shown that most modes are stabilized except the very short and slowly growing modes.

5.0 Publications Resulting from This Research

Refereed Journals

1) "Microwave Growth from the Beam Breakup Instability in Long-Pulse Electron Beam Experiments", P. R. Menge, R. M. Gilgenbach, and R.A. Bosch, Applied Physics Letters, (in press for August 10, 1992)

2) "The Beam Breakup Instability in Quadrupole and Solenoidal Electron Beam Transport Systems", R.A. Bosch, P.R. Menge, and R.M. Gilgenbach, Journal of Applied Physics, 71 (1992)

Conference Papers

1) "Experiments on the Excitation and Coupled-Cavity Suppression of Beam Breakup Instability in Long-Pulse Electron Beam Transport", R. M. Gilgenbach, P.R. Menge, M.T. Walter, C. H. Ching, J. Foster, and P.L.G. Ventzek, Presented at Beams '92, In Washington, D.C., May 25-29, 1992

2) "Beam Breakup Instability Experiments on Long Pulse Electron Beam Transport Through RF Cavities", P.R. Menge, R. M. Gilgenbach, H. Ching, T.A. Spencer, and M. Walter, Presented at the SPIE's OE-LASE'92, January 1992, Los Angeles, CA

3) "Experiments on Long-Pulse Electron Beam Breakup Instability in RF Cavities with Solenoidal Focusing", P.R. Menge, R.M. Gilgenbach, R.A. Bosch, C.H. Ching, and T.A. Spencer, Presented at the 1991 Annual Meeting of the Division of Plasma Physics of the American Physical Society, Nov. 4-8, 1991, Tampa, Florida

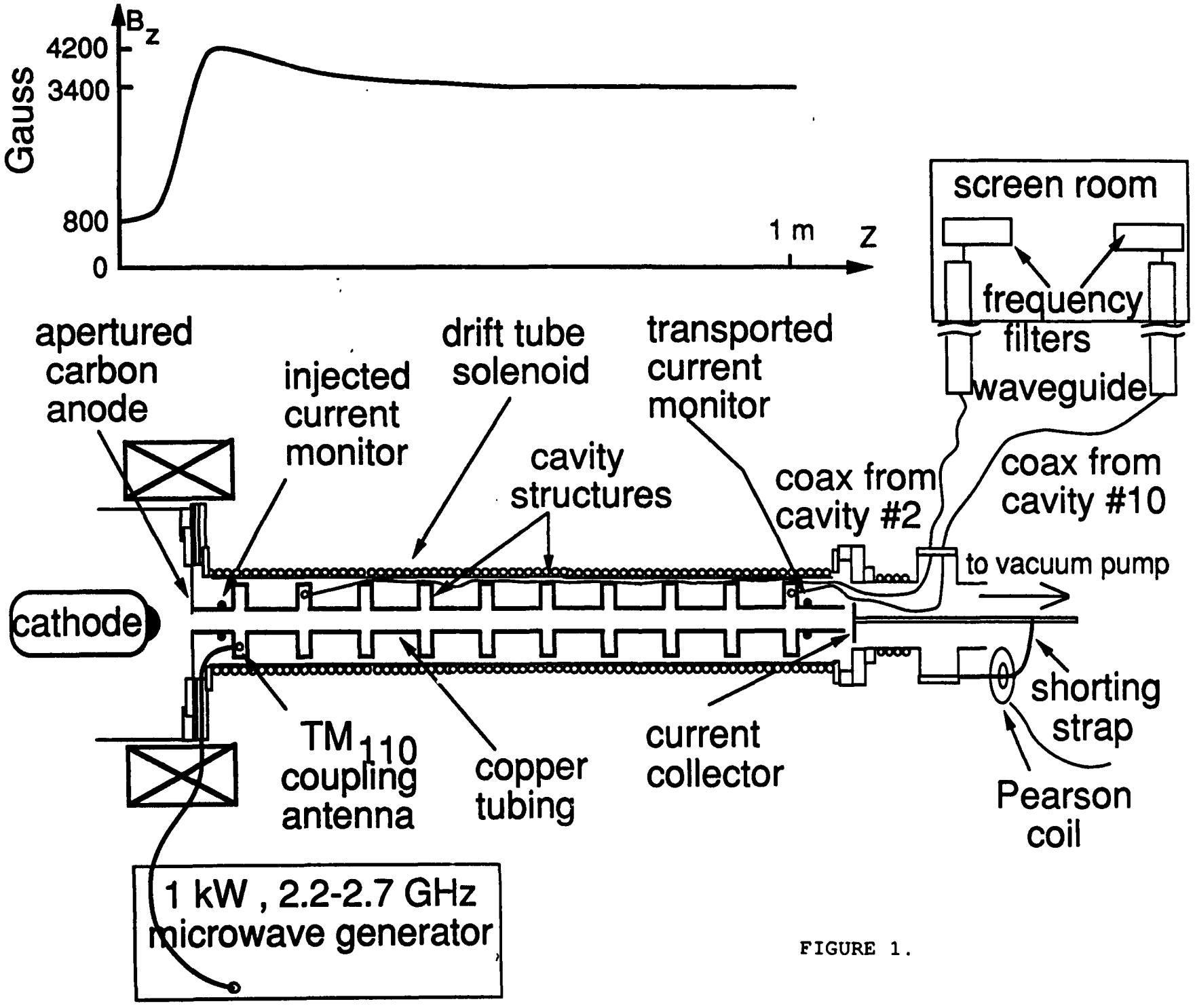
B_z
4200
3400
Gauss
800
0
1 m
z
screen room
frequency
filters
waveguide
apertured
carbon
anode
injected
current
monitor
drift tube
solenoid
transported
current
monitor
cavity
structures
coax from
cavity #2
coax from
cavity #10
to vacuum pump
cathode
shorting
strap
TM 110
coupling
antenna
copper
tubing
current
collector
Pearson
coil
1 kW , 2.2-2.7 GHz
microwave generator

FIGURE 1.

RF Growth vs. Ratio of Current to Magnetic Field

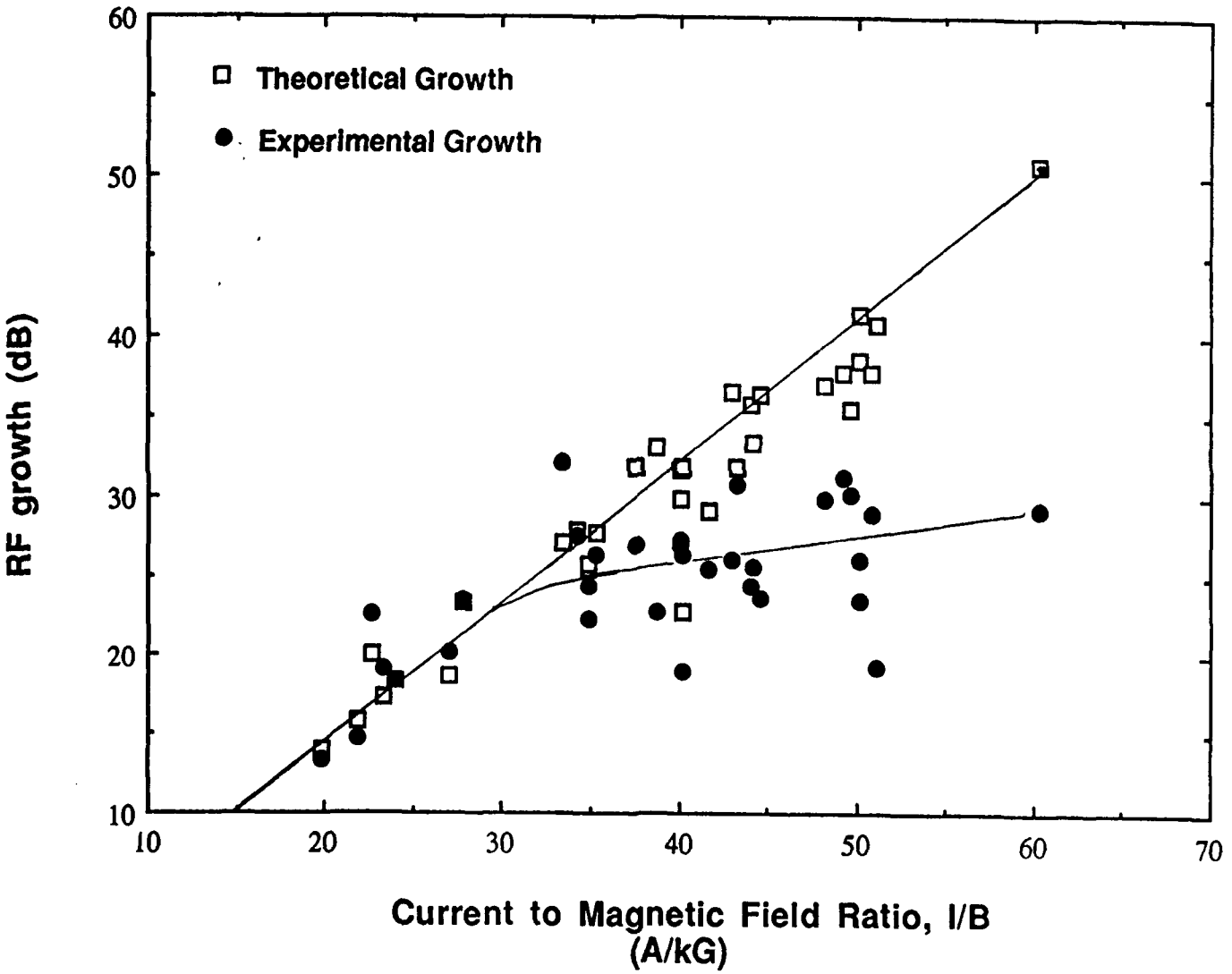

Figure 2

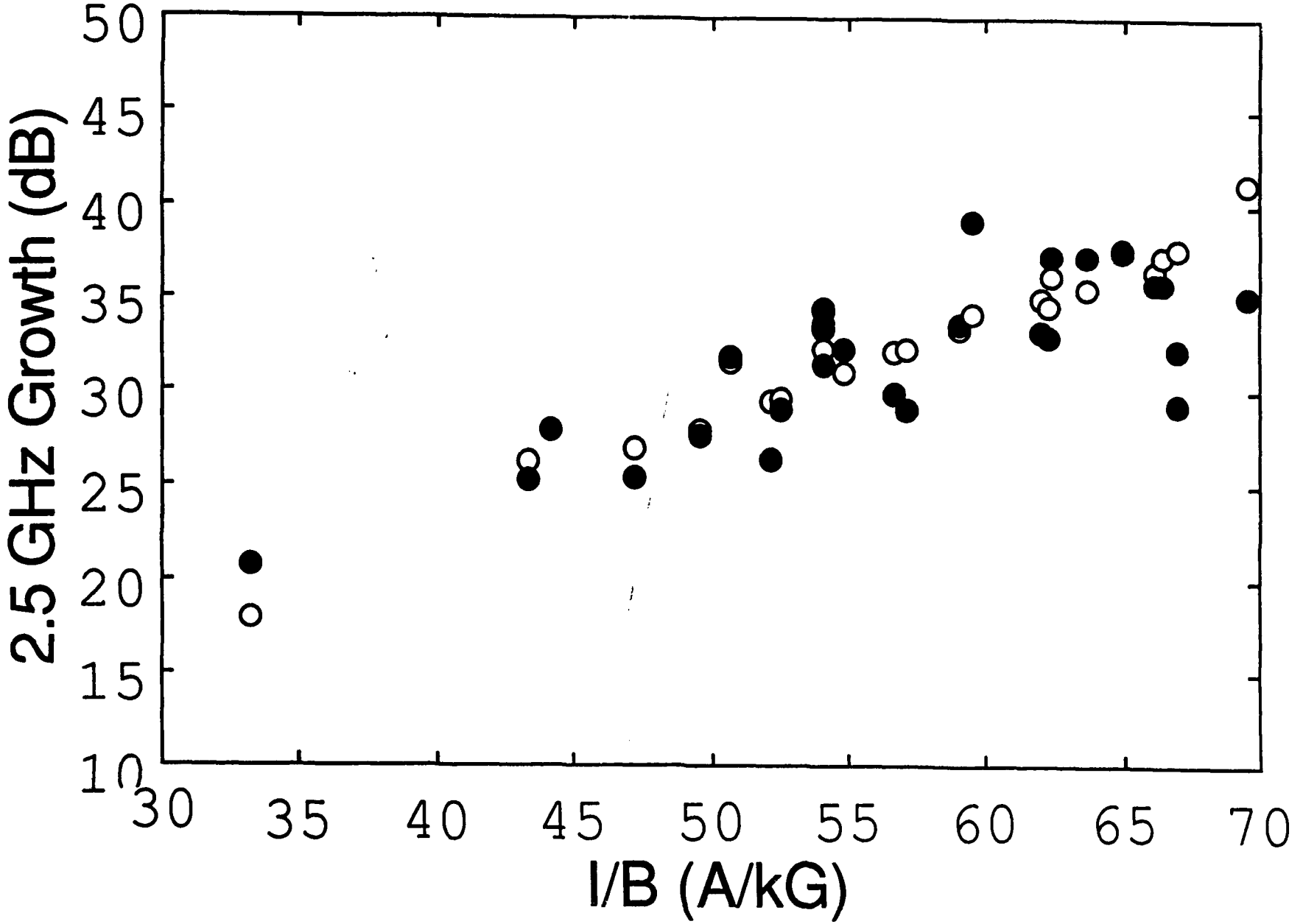
2.5 GHz Growth (dB)
50
45
40
35
30
25
20
15
10
30
35
40
45
50
55
60
65
70
I/B (A/kG)

FIGURE 3.

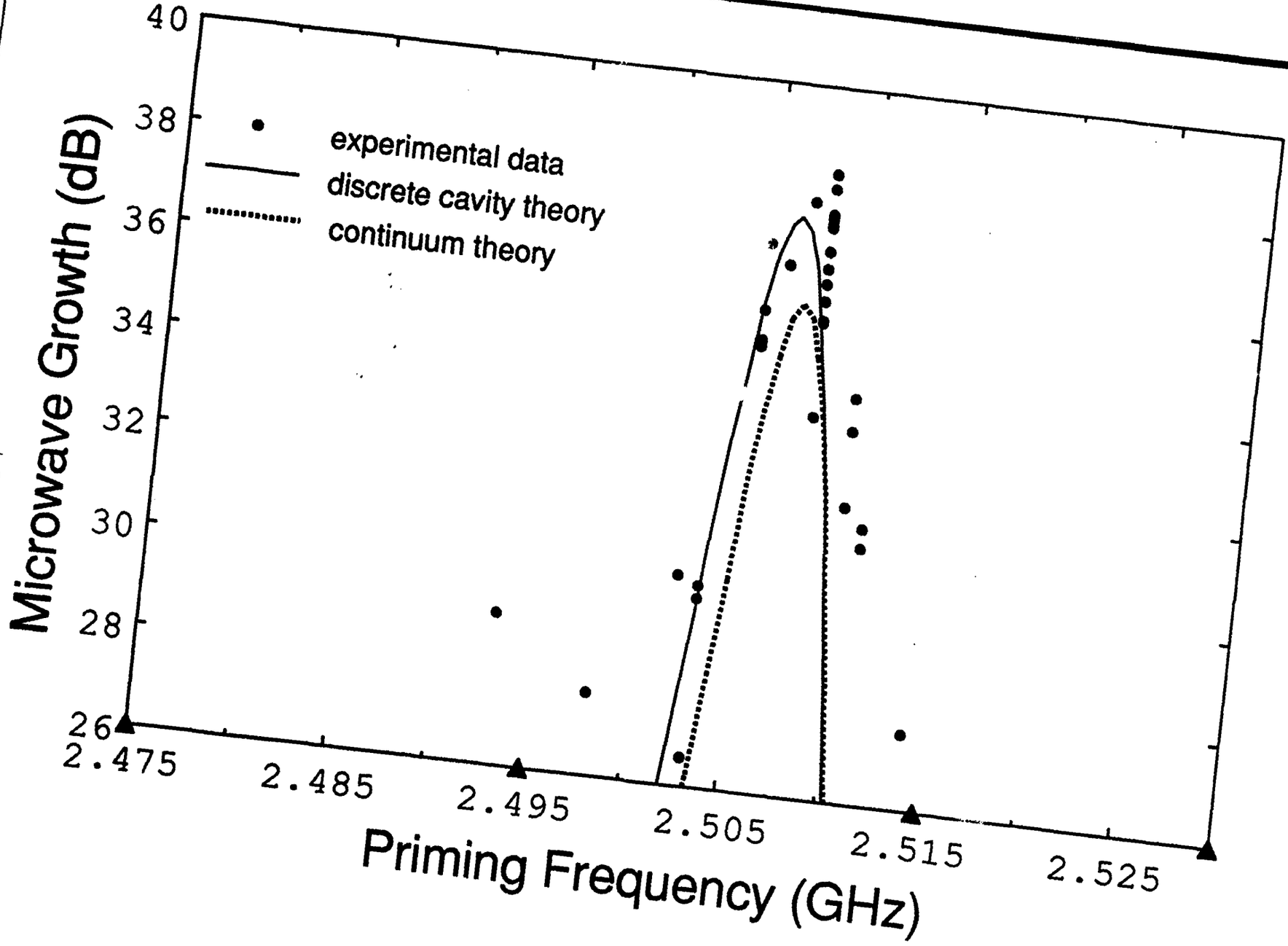
40
38
36
34
32
30
28
26
Microwave Growth (dB)
experimental data
discrete cavity theory
continuum theory
2.475
2.485
2.495
2.505
2.515
2.525
Priming Frequency (GHz)

FIGURE 4.

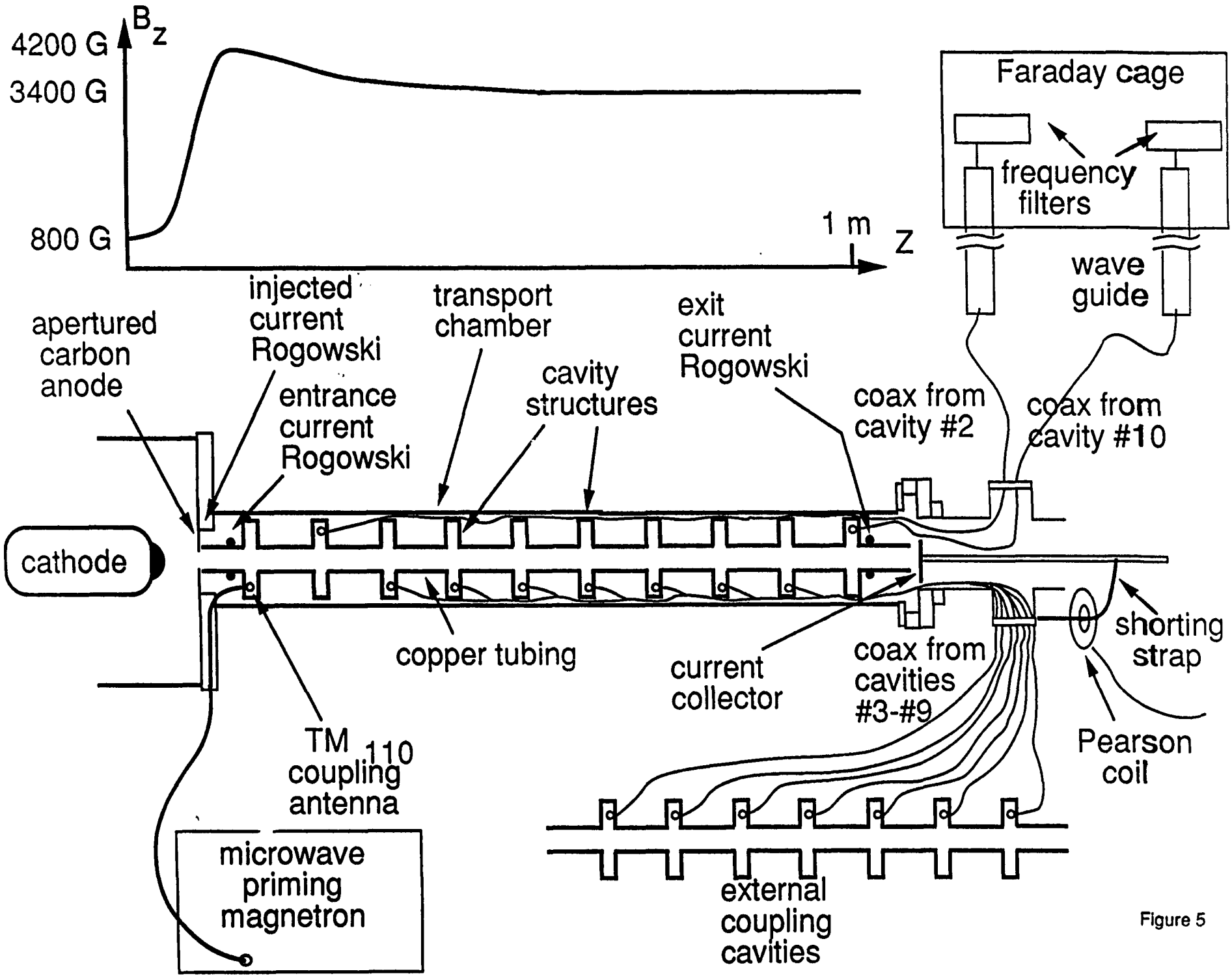
4200 G
3400 G
800 G
B_z
1 m
z
Faraday cage
frequency filters
wave guide
injected current Rogowski
transport chamber
exit current Rogowski
apertured carbon anode
entrance current Rogowski
cavity structures
coax from cavity #2
coax from cavity #10
cathode
copper tubing
current collector
coax from cavities #3-#9
shorting strap
Pearson coil
TM 110 coupling antenna
microwave priming magnetron
external coupling cavities

Figure 5

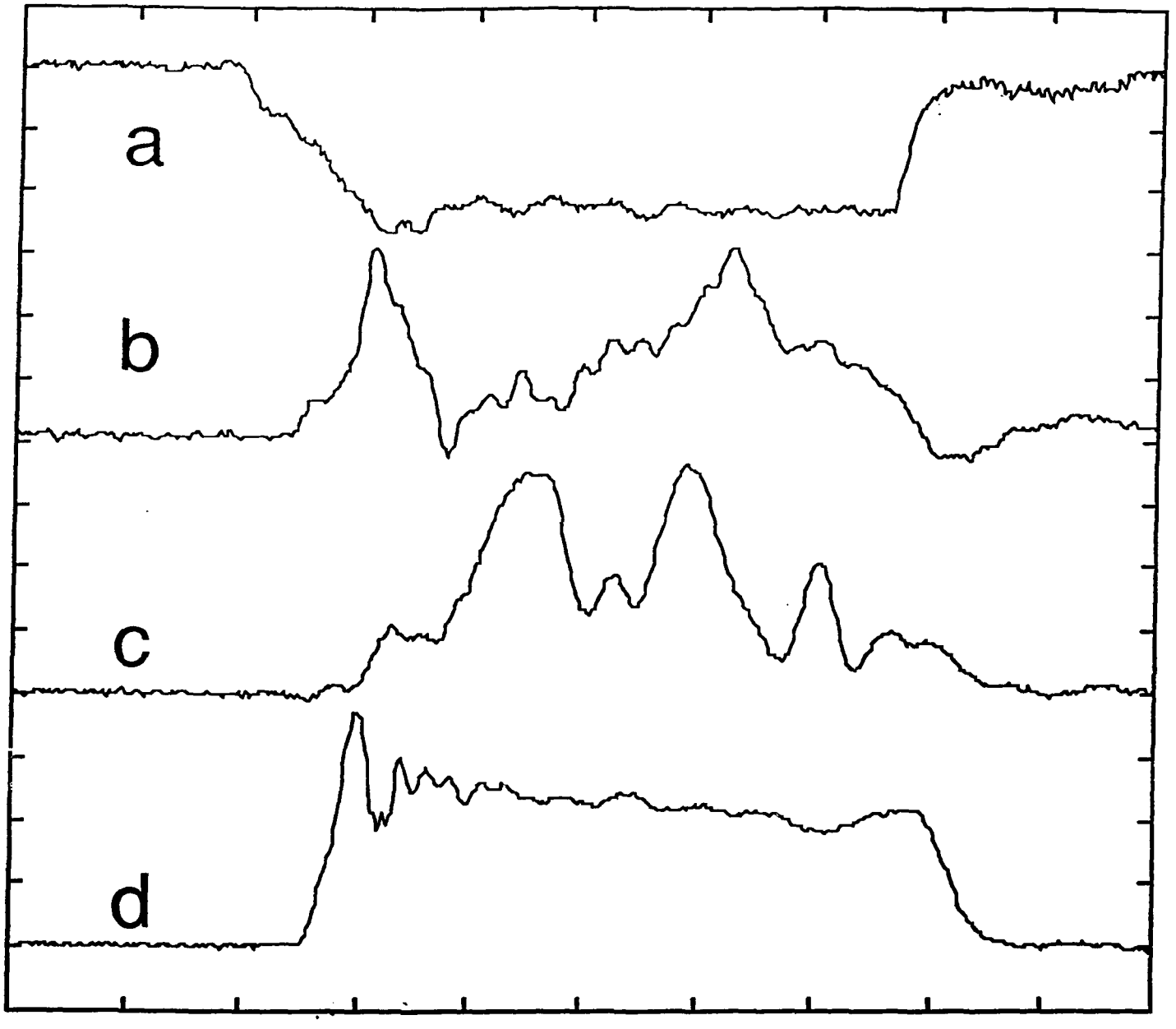

Figure 6 Experimental data for uncoupled cavities: (a) Electron beam voltage (310 kV/div); (b) Microwave diode detector signal in the second cavity, filtered at 2.5075 ± 0.0115 GHz (50 mV/div); (c) Microwave diode detector signal in the tenth cavity filtered at 2.5075 ± 0.0115 GHz with 36 dB attenuation (50 mV/div); (d) Transported current leaving tenth cavity (92 A/div) from a different shot. Applied solenoid field is 3.4 kG.

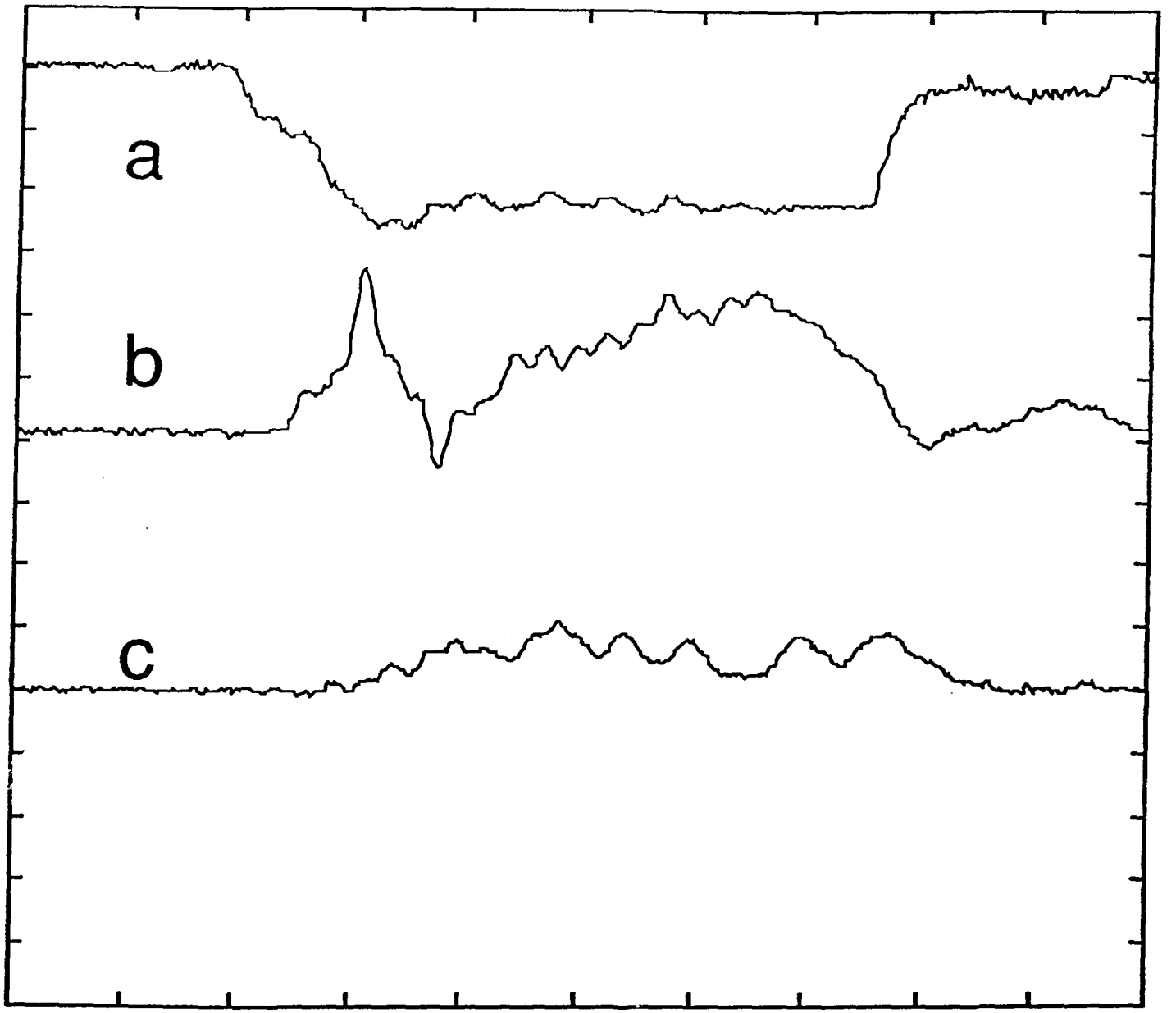

Figure 7. Experimental data for externally coupled cavities: (a) Electron beam voltage (310 kV/div); (b) Microwave diode detector signal in the second cavity, filtered at 2.5075 ± 0.0115 GHz (50 mV/div); (c) Microwave diode detector signal in the tenth cavity filtered at 2.5075 ± 0.0115 GHz with 36 dB attenuation (50 mV/div). Applied solenoid field is 3.4 kG.

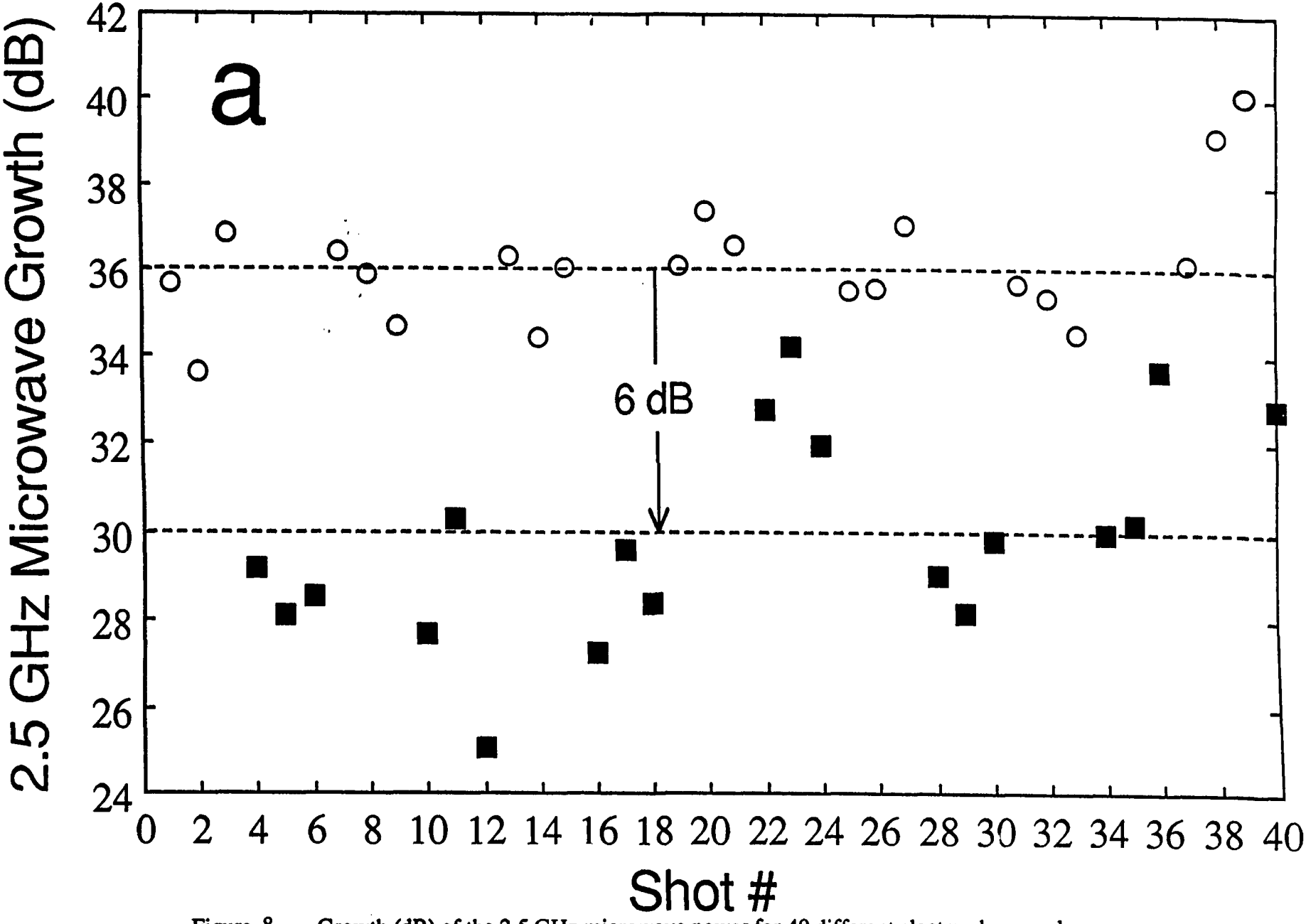

Figure 8. Growth (dB) of the 2.5 GHz microwave power for 40 different electron beam pulses showing uncoupled shots (open circles) and externally coupled shots (filled squares).

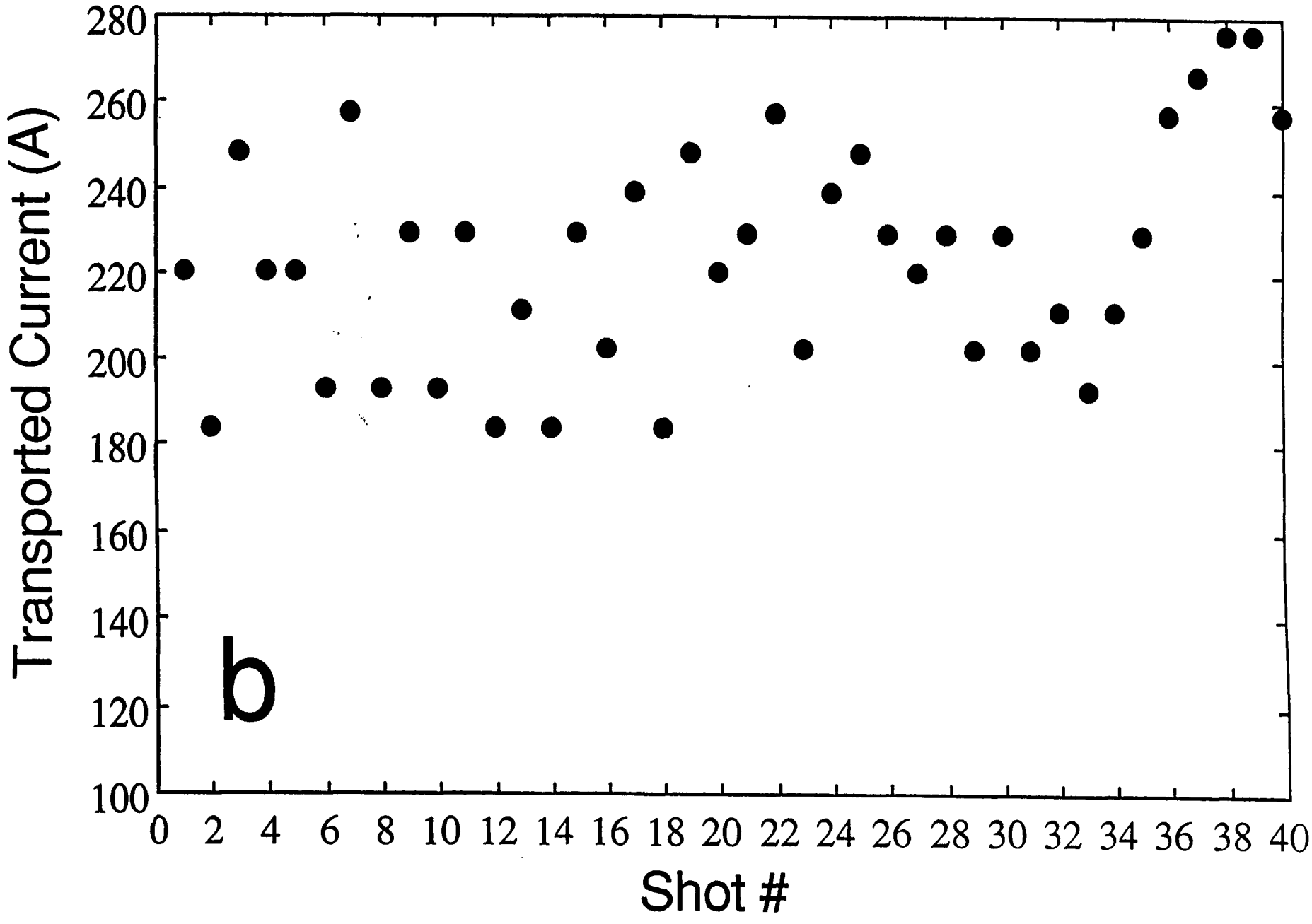

Figure 9 Transported electron beam current (A) for the corresponding shot numbers of 8.

Microwave growth from the beam breakup instability in long-pulse electron beam experiments

Page proof

P. R. Menge, R. M. Gilgenbach, and R. A. Bosch
Intense Energy Beam Interaction Laboratory, Nuclear Engineering Department, University of Michigan, Ann Arbor, Michigan 48109-2104

(Received 2 April 1992; accepted for publication 8 June 1992)

The beam breakup (BBU) instability has been investigated in high-current, long-pulse electron beams propagating through microwave cavities. Experiments are performed using a relativistic electron-beam generator with diode parameters: 0.7–0.8 MV, 1–15 kA, and 0.5–1.5 μs. The magnitude of the solenoidal magnetic field places these experiments in an intermediate regime between strong focusing and weak focusing. The electron-beam transport system consists of ten identical pillbox cavities each containing a small microwave loop antenna designed to detect the TM_{110} beam breakup mode. The TM_{110} microwave mode is primed in the first cavity by a magnetron tuned to the resonance frequency of 2.5 GHz. The BBU instability growth is measured through the amplification of the 2.5 GHz microwaves between the second and tenth cavities. Strong growth (25–38 dB) of the TM_{110} microwave signal is observed when the initial cavity is primed exactly on resonance, with a rapid decrease of the growth rate off-resonance. The magnitude of microwave growth is consistent with the predictions of BBU theory.

The beam breakup (BBU) instability is one of the most serious instabilities in high-current and long-pulse electron-beam accelerators. The BBU instability results from the coupling between the transverse motions of the electron beam and the nonaxisymmetric TM_{110} mode of the cavity structure.[1] This important instability can cause numerous effects on electron beams, such as emittance degradation, loss of current, and pulse shortening.[2,3] Recently, there has been interest in using transverse e-beam modulation to produce high-power microwaves.[4–7] While the theory of the BBU instability has been advanced considerably in recent years,[8–13] there have been few journal publications where BBU is systematically studied in experiments and compared with theories.[14]

In this letter, we study the evolution of BBU instability in a few (ten) cavity system. This problem is of interest in multicavity klystrons and magnicons,[15] and may serve as a stringent test of the continuum description of BBU in a few-cavity system. The present experimental approach utilizes a long-pulse electron beam coasting through a series of identical microwave cavities. The first cavity is primed at the TM_{110} resonance frequency by a kilowatt microwave magnetron. The parameters for these experiments place the BBU growth rate scaling close to the boundary between the weak[1] and strong focusing[9,16] regimes (defined in Ref. 3).

The electron-beam accelerator used for the experiments is the Michigan Electron Long Beam Accelerator (MELBA) with diode parameters: voltage $= -0.7$–0.8 MV, current $= 1$–15 kA, and pulse length $= 0.5$–5 μs, with voltage flattop provided by an Abramayan-type compensation stage over 1.5 μs.[17]

The experimental configuration is shown is Fig. 1. The electron beam is produced by a field/explosive emission button cathode. The cathode is covered with cotton velvet and is mounted on a hemispherical-end cathode stalk. The anode consists of a graphite plate located 10.8 cm from the end of the cathode. Centered in the anode is a circular aperture (2-cm diameter) which extracts 40–300 A into the transport chamber. The diode chamber is immersed in a uniform solenoidal magnetic field that can be varied from 0.5–1.2 kG.

The transport chamber consists of a stainless-steel vacuum drift tube wound with solenoidal coils pulsed independently from the diode. These coils produce a quasi-dc magnetic field of up to 3.5 kG (duration = 20 ms). Figure 1 (upper) illustrates the magnetic-field profile of the experiment. Within the drift tube are ten brass pillbox resonant cavities with a radius of 6.9 cm and a length of 2.0 cm. Inside each cavity is a small loop antenna (0.7-cm diameter) oriented to be sensitive to the TM_{110} cavity mode. The average TM_{110} resonant frequency is 2.5075 ± 0.0026 GHz, and the average Q is 215 ± 45. These low-Q values were obtained by loading each cavity with a ring of microwave absorber. The cavities are separated by smaller diameter copper tubes (radius = 1.9 cm, length = 6.5 cm). The purpose of these tubes is to cutoff the electromagnetic propagation of the microwaves in the cavities. Thus, there is negligible cavity-to-cavity crosstalk and the system is immune to the regenerative BBU instability. The measured attenuation of the 2.5 GHz, TM_{110} microwave is 26 dB from cavity-to-adjacent cavity.

The loop antenna in the first cavity is connected to a 1-kW level external microwave pulse generator (magnetron) to prime the cavity's TM_{110} mode. The priming microwave pulse is 3-μs long and begins before the e beam is present. In the second cavity, the e beam-induced microwave signal is received by the loop antenna and propagated out of the vacuum chamber through coaxial cable to an S-band waveguide. At the end of the waveguide, the microwave signal is attenuated and filtered for frequency information. Part of the microwave signal is diverted into a filter which passes 2.5075 ± 0.0115 GHz. The filter rejects all frequencies except that which corresponds to the TM_{110} beam breakup mode. The microwave power is measured with diode detectors. The rf in the tenth and last cavity is

 0003-6951/92/310001-03$03.00 © 1992 American Institute of Physics

A-1

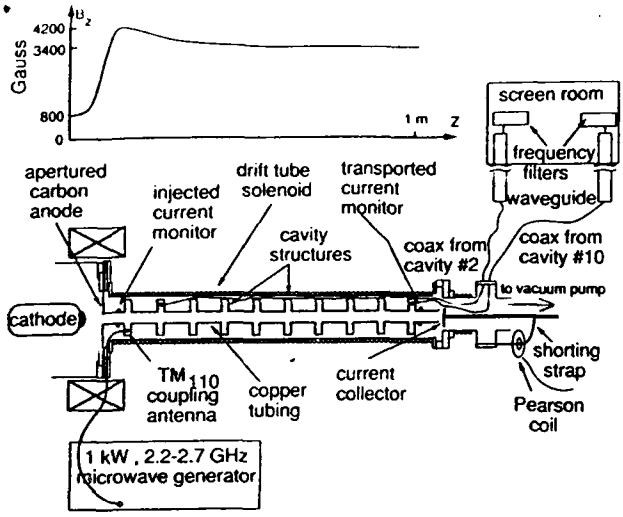

FIG. 1. Experimental configuration (lower), with typical magnetic-field profile (upper).

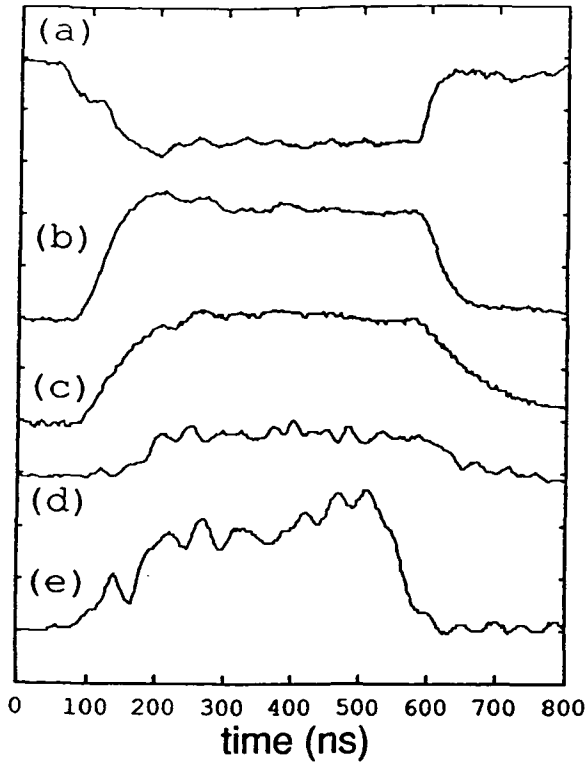

FIG. 2. Experimental data: (a) Electron beam (465 kV/div); (b) injected current into first cavity (92 A/div); (c) transported current leaving tenth cavity (92 A/div); (d) microwave diode detector signal in the second cavity, filtered at 2.5075 ± 0.0115 GHz, 6-dB attenuation; (e) microwave diode detector signal in the tenth cavity filtered at 2.5075 ± 0.0115 GHz, 35-dB attenuation.

measured in the same way with its own cable, waveguide, and filter. The BBU growth is determined by the decibels of growth in 2.5-GHz microwave power between the second and tenth cavities.

The beam current is measured before entering the first cavity and after exiting the last cavity using calibrated Rogowski coils. After exiting the cavity structure, the beam propagation is terminated by a copper collector plate grounded by a cable which passes through a Pearson current transformer.

Figure 2 depicts typical experimental data. The uppermost trace (a) is the MELBA diode voltage in which the flattop occurs at 750 kV and lasts for 600 ns. The second signal (b) is the current entering the first cavity with a peak which corresponds to 200 A. Signal (c) is the current exiting the tenth cavity, and the peak corresponds to 190 A. The fourth signal (d) is the microwave power signal in the second cavity after being filtered at 2.5 GHz; the signal has been attenuated by 6 dB. The lowermost signal (e) is the microwave power in the tenth cavity after being filtered at 2.5 GHz; this signal has been attenuated by 35 dB. Allowing for the difference in signal amplitudes and detector sensitivities, the growth of the 2.5-GHz microwaves is measured to be about 36 or 4.5 dB per cavity. This data was taken at a solenoidal magnetic field of 3.4 kG.

The theoretical magnitude of beam breakup instability growth can be obtained by calculating the imaginary wavenumber in the BBU dispersion relation. If the continuum theory[3,18] is used the appropriate dispersion relation is

$$(\Omega^2-\omega_c\Omega+\Gamma)\ (\Omega^2+\omega_c\Omega+\Gamma)=0, \qquad (1)$$

where, $\Omega=\omega-\nu k$

$$\Gamma=\frac{2\omega_0^4\epsilon}{-\omega^2+\omega_0^2+i\omega\omega_0/Q},$$

ω_c is the relativistic betatron frequency, ω is the frequency of the beam breakup wave, ν is the velocity of the electron beam, k is the wavenumber, ω_0 is the angular frequency of the TM_{110} mode, Q is the quality factor of the cavity, and ϵ is the dimensionless coupling factor.[19] Using the data from Fig. 2, the calculated BBU growth is 34 dB.

If the betatron wavelength or the BBU e-folding length does not generally exceed the spacing of the accelerator cavities, then the transverse impulsive forces from the cavities can no longer be treated as a continuous force per unit length. If this condition exists, then a continuum model may be inappropriate, and a model treating the cavities as discrete entities would be more applicable. This is the case here, for the betatron wavelength of the MELBA beam at 3.4 kG is 7.8 cm, and the cavity spacing is 8.5 cm. Thus, a more accurate dispersion relation is[20]

$$k(\omega)=\frac{\omega}{\nu}\pm\frac{\omega_c}{2\nu}-\frac{1}{L}\arccos\left(\cos\frac{L\omega_c}{2\nu}+\frac{\Gamma L}{\omega_c\nu}\sin\frac{L\omega_c}{2\nu}\right), \qquad (2)$$

where L is the distance between adjacent cavity centers. Using the data from Fig. 2, the calculated growth rate is 35 dB for the discrete-cavity asssumption.

Figure 3 shows the 2.5-GHz microwave signal growth plotted for various values of I/B (I/B is the ratio of transported current to the magnetic field). The theoretical BBU growth rate is approximately linearly proportional to I/B. The solid circles are experimental data which were obtained by varying the magnetic field. The open circles are the discrete-clarity [Eq. (2)] theoretical growth points as calculated from the parameters of the corresponding ex-

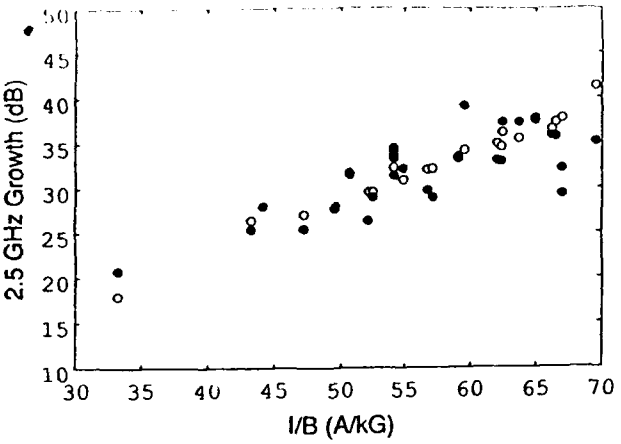

FIG. 3. Microwave growth (2.5 GHz) dependence on the current to magnetic-field ratio, I/B. The filled circles are experimental data and the open circles are theoretical predictions calculated by the discrete-cavity theory [Eq. (2)] from the corresponding experimental points with the same I/B.

perimental points. The values of ϵ for the plotted points range from 5.6×10^{-5} to 5.2×10^{-4}. The agreement between theory and experiment is excellent at low currents. The larger difference between theory and experiment at higher currents could be due to e-beam-induced detuning of the cavity resonance from its cold-test value.[14]

Figure 4 shows the effect of the priming the first cavity at frequencies other than its exact TM_{110} mode resonant frequency. The plotted points are experimental data taken at the same magnetic field (3.4 kG) and nearly the same e-beam current (190–215 A). The solid curve is the BBU growth as predicted by the discrete-cavity equation (2) using $I=210$ A and letting ω vary as the priming angular frequency. The dashed curve is the continuum BBU growth equation (1) for the same parameters. This experimental data is strongly peaked near the central TM_{110} resonant frequency of 2.5075 GHz, showing that this

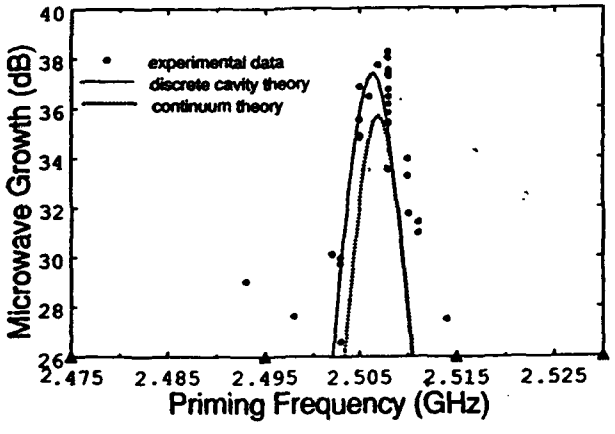

FIG. 4. Microwave growth dependence on the frequency of microwaves injected into the first cavity. The filled circles are experimental data. The solid curve is the theoretical growth predicted by the discrete-cavity mode coupled theory, Eq. (2) (see Ref. 20). The dashed curve is the theoretical growth predicted by the continuum cavity mode coupled theory, Eq. (1) (see Refs. 3 and 18). The triangles along the abscissa indicate experimental growth below the level of detectability (i.e., below 26 dB).

mode, and thus, the beam breakup instability, is responsible for the observed microwave growth. It should be noted that the experimental beam breakup instability growth more closely follows the discrete-cavity theory than the continuum theory. This expected because the continuum theory assumes that the distance between cavities is negligible compared to the betatron wavelength and the BBU e-folding length. For this experiment, both the betatron wavelength and the e-folding length are compared to the distance between cavity centers.

In conclusion, the beam breakup instability has been experimentally studied for the difficult regime of intermediate focal strength. The adequacy of the continuum BBU description for few-cavity systems is tested, even under conditions where the betatron wavelength is comparable to the cavity spacing. Strong instability growth is only found by microwave priming at the resonance frequency of the TM_{110} microwave mode, a characteristic of the beam breakup instability.

We appreciate valuable discussions with Y. Y. Lau of the Naval Research Laboratory. We acknowledge the experimental assistance of P. L. G. Ventzek, C. H. Ching, M. Walter, J. Forster, and T. Spencer. This research was supported by SDIO-IST through an ONR contract.

[1] W. K. H. Panofsky and M. Bander, Rev. Sci. Instrum. 39, 206 (1968).
[2] R. Helm and G. Loew, *Linear Accelerators*, edited by P. M. Lapostelle and A. L. Septier (North Holland, Amsterdam, 1970), Chap. B.1. 4, p. 173.
[3] Y. Y. Lau, Phys. Rev. Lett. 63, 1141 (1989).
[4] B. B. Godfrey, D. J. Sullivan, M. J. Arman, T. C. Genoni, and J. E. Walsh, Proc. SPIE Int. Soc. Opt. Eng. 1061, 84 (1989).
[5] Thomas J. T. Kwan, Michael A. Monstrom, and Brendan B. Godfrey, Phys. Rev. Lett. 66, 3221 (1991).
[6] P. J. Tallerico, IEEE Electron. Dev. ED-26, 1559 (1979).
[7] R. J. Adler, J. R. Bayless, S. Humphries, Jr., and George A. Proulx, Pulse Sciences, Inc., San Leandro, CA, Report PSI-FR-2293-1 (1988).
[8] V. K. Neil and R. K. Cooper, Part. Accel. 1, 111 (1970).
[9] V. K. Neil, L. S. Hall, and R. K. Cooper, Part. Accel. 9, 213 (1979).
[10] A. W. Chao, B. Richter, and C. Y. Yao, Nucl. Instrum. Methods 178, 1 (1980).
[11] R. L. Gluckstern, R. K. Cooper, and P. J. Channell, Part. Accel. 16, 125 (1985).
[12] D. G. Colombant and Y. Y. Lau, Appl. Phys. Lett. 55, 27 (1989).
[13] C. L. Bohn and J. R. Delayen, in Conference Record of *1991 IEEE Particle Accelerator Conference*, IEEE Catalogue No. 91 CH3038-7, 3, 1809 (1991).
[14] P. R. Menge, R. M. Gilgenbach, R. A. Bosch, H. Ching, T. A. Spencer, and M. Walter in *Intense Microwaves and Particle Beams III*, H. E. Brandt, Editor, Proc. SPIE 1629, 529 (SPIE, Bellingham, WA, 1992).
[15] S. Gold, private communication.
[16] G. J. Caporaso, F. Rainer, W. E. Martin, D. S. Prono, and A. G. Cole, Phys. Rev. Lett. 57, 1591 (1986).
[17] R. M. Gilgenbach, L. D. Horton, R. F. Lucey, Jr., S. Bidwell, M. Cuneo, J. Miller, and L. Smutek, in *Digest of the 5th IEEE Pulsed Power Conference* (IEEE, New York, NY, 1985), p. 126.
[18] R. A. Bosch and R. M. Gilgenbach, Appl. Phys. Lett. 58, 699 (1991).
[19] The epsilon factor for the TM_{110} mode is $\epsilon=0.422(l/L)[I(kA)/17](\beta/\gamma)$, where l is the cavity length, L is the cavity spacing, I is the beam current, and β and γ are the usual relativistic velocity and mass factors. See Refs. 3 and 12 for further explanation.
[20] R. A. Bosch, P. R. Menge, and R. M. Gilgenbach, J. Appl. Phys. 71, 3091 (1992).

A-3

To be published in conference proceedings of Beams 92 May 25 - 29, 1992

EXPERIMENTS ON THE EXCITATION AND COUPLED-CAVITY SUPPRESSION OF BEAM-BREAKUP-INSTABILITY IN LONG-PULSE ELECTRON BEAM TRANSPORT

R. M. GILGENBACH, P. R. MENGE, M. T. WALTER,
C. H. CHING, J. FOSTER, and P.L.G. VENTZEK
Intense Energy Beam Interaction Laboratory
Nuclear Engineering Department
University of Michigan
Ann Arbor, MI 48109-2104

Abstract

Experiments have been performed to excite and suppress the beam breakup (BBU) instability in long pulse electron beam transport through RF cavity systems. Electron beams are generated by the Michigan Electron Long Beam Accelerator (MELBA) at parameters: V=0.7-0.8 MV, I_{diode} = 1-10 kA, $I_{injected}$ = 100-400 A, and pulselength= 0.5-1 μs. The transport system consists of a solenoidal magnetic field with 10 RF cavities. The TM_{110} mode BBU resonance frequency of the cavities is 2.5 GHz and the cavity Q is adjusted to about 200-300. Each cavity has a small coupling loop oriented to detect the RF field in the TM_{110} mode. The cavities are separated by 6.5 cm-long sections of tubing which are cutoff to the RF frequency. The BBU instability is primed by a kW level microwave signal injected into the first cavity from a magnetron. Growth of the RF is measured between the second cavity and the last cavity. Strong growth (2-5 dB per cavity) is only observed when the RF priming signal is tuned to the exact TM_{110} mode resonance frequency ($\Delta f/f_0 << 1\%$). Experiments to test techniques for suppression of the BBU instability are also being performed. The primary BBU suppression technique being investigated is cavity cross-coupling, in which 7 out of 10 internal beam-cavities are connected by cables to 7 identical cavities located externally to the e-beam. These are the first experiments which have shown a consistent reduction (about -6 dB average) in BBU microwave growth when external cavities are coupled to the internal cavity system.

Introduction

The beam breakup instability is the most serious instability which limits the pulselength and current of electron accelerators.[1] Beam breakup instability can also be a problem in multi-cavity klystrons. During the past several years a great deal of theoretical research has advanced the knowledge of the BBU[1-5]. Very few experiments to-date have systematically excited the BBU in high current, long-pulse electron beams. Experiments at the University of Michigan have the goal of exciting the beam breakup instability on a few (ten) cavity system and measuring the scaling of BBU growth.[6,7] Suppression techniques for the BBU are also being investigated, particularly coupled-cavities.[8,9] These experiments are made possible by an accelerator which operates at long-pulse and high current; the Michigan Electron Long Beam Accelerator[10], MELBA, operates at diode parameters of 0.7-0.8 MV, 1-10 kA, and pulselength of 0.5-1 μs. The parameters of this electron beam transport experiment are in a unique regime[2], intermediate between previous weak focusing[1] and strong focusing[3,4] regimes.

Experimental Configuration

The experimental configuration for the beam breakup instability growth measurement is depicted in Figure 1. The experiment is driven by the MELBA accelerator,[10] which is based on a Marx generator with an Abramyan type compensation stage, which flattens the voltage over pulselengths of about 1 μs. Pulselengths on MELBA can be set by an adjustable crowbar switch between 0.3-1 μs and are typically set at about 0.5 μs for these experiments. A velvet button cathode is installed on the hemispherical end of the cathode stalk. A graphite aperture defines the 2-cm injected beam diameter and yields extracted currents of 40-400 A. The anode cathode gap is about 10.2 cm. Diode magnetic field (≈0.8 kG) is generated by large coils pulsed by a capacitor bank. The transport chamber is a stainless steel tube wound with pulsed solenoidal magnetic field coils. Typical solenoidal magnetic fields of 3-4 kG were employed.

Inside the chamber is an array of ten brass pillbox microwave cavities with radius of 6.9 cm and length of 2.0 cm. The TM_{110} mode resonant frequency of each cavity is set at 2.5075 GHz ± 0.0026 GHz. In order to lower the cavity Qs to values of about 200-300, each cavity was loaded with a small ring of microwave absorber. Smaller radius (1.9 cm) copper tubes of length 6.5 cm connect the cavities and prevent electromagnetic crosstalk (-26 dB), which would lead to the regenerative BBU instability.

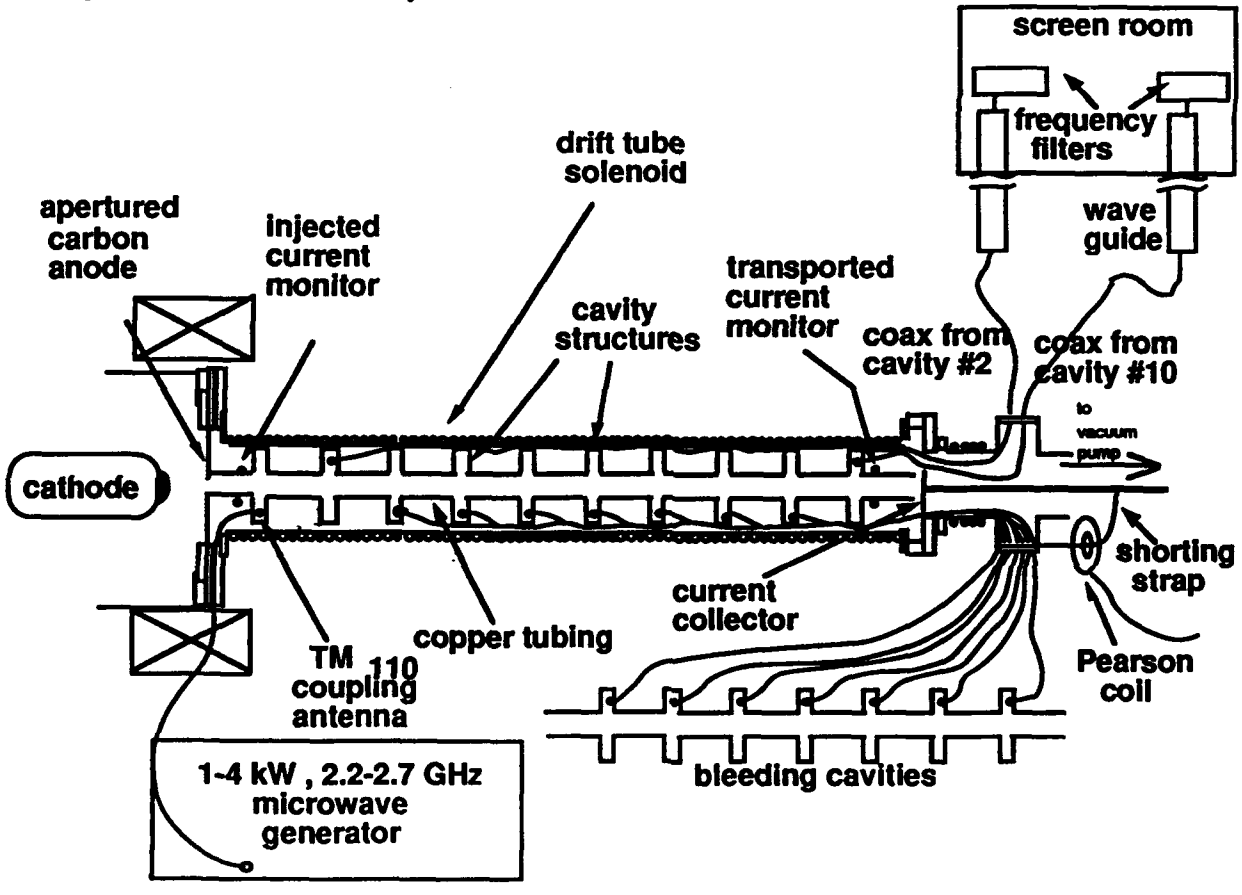

Figure 1. Experimental Configuration

Each cavity contains a small coupling loop designed to detect the TM_{110} mode for cold-testing and e-beam experiments. The coupling loop in the first cavity is utilized for priming the TM_{110} mode with the signal from a kW level microwave pulse generator. Coupling loops in the second and tenth cavities are used to measure the growth of beam-breakup-instability -generated microwaves as the electron beam coasts through the cavity system. Microwave signals are coupled out of the chamber by coaxial cable and transmitted to the Faraday cage by waveguide. In the Faraday cage, the signals are filtered to extract the BBU signal at the TM_{110} mode resonance frequency of 2.5075 ± 0.0115 GHz and signals are attenuated for measurement on crystal detectors. For coupled-cavity BBU growth experiments, a set of equal-length (16λ) coaxial cables connects seven internal cavities to seven identical external cavities. For baseline BBU growth measurements, the coaxial cables are disconnected between internal and external cavities.

Electron beam current is measured at a number of points in the transport experiment. Cathode stalk current in the diode is measured by a B-dot loop in the MELBA oil tank, behind the insulators. Extracted current is monitored by a Rogowski coil in the flange after the anode. Injected current is measured by a Rogowski coil before the first cavity and exit current is detected by a Rogowski coil after the last cavity. Exiting current is also measured by a current collector which is grounded by a strap which passes through a Pearson current transformer.

Experimental Results

In order to compare the BBU growth for the uncoupled-cavity baseline case to the coupled-cavity case, a typical experimental run alternated between several shots for each case. Microwave priming was applied to the first cavity for several microseconds before the e-beam pulse. The solenoidal magnetic field was about 3.4 kG. Experimental data signals for microwave priming of the beam-breakup-instability for the baseline case (no external coupled cavities) are presented in Figure 2. The voltage flattop was reached after about 200 ns, at which time the electron beam current was nearly flat. In Figure 2, the baseline (uncoupled-cavity) microwave growth is about 36 dB between the second cavity signal and the tenth cavity signal. Injected electron beam current was typically about 200-300 A; 75-90% of this current was transported through the 10 cavity system.

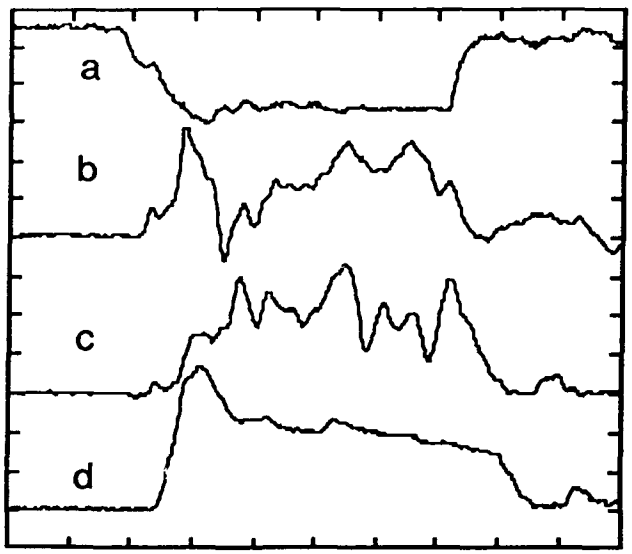

Figure 2. Uncoupled cavity data. (a) Diode voltage (310 kV/div). (b) 2nd cavity 2.5 GHz diode detector signal (50 mV/div). (c) 10th cavity diode detector signal (50 mV/div). (d) Transported current (92 A/div) from a different shot. The applied magnetic field is 3.4 kG.

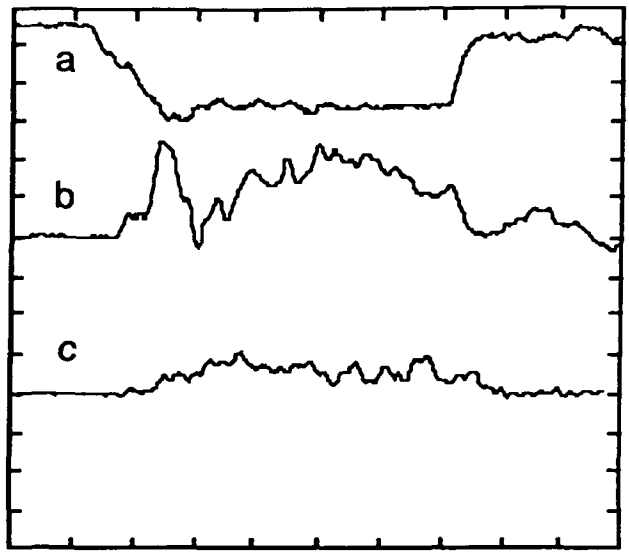

Figure 3. Coupled cavity data. (a) Diode voltage (310 kV/div). (b) 2nd cavity 2.5 GHz diode detector signal (50 mV/div). (c) 10th cavity diode detector signal (50 mV/div). The applied magnetic field is 3.4 kG.

For comparison, data from a coupled cavity shot is presented in Figure 3; in this case, the microwave growth between the two signals is much lower, about 25 dB. A summary of beam-breakup-instability microwave growth data from some 40 shots is presented in Figure 4. The data show a consistent reduction of BBU growth from about 36 dB average ($\sigma = \pm$ 1.5 dB) for the uncoupled case to about 30 dB average ($\sigma = \pm$ 2.4 dB) for the coupled-cavity case. Thus, for the present seven cavity system, we measure an average BBU growth reduction of about 6 dB due to coupled-cavities. Variations of BBU signal amplitudes may be due to varying current amplitudes and other differences between shots. Figure 5 presents the transported current for each pulse of Figure 4. A correlation can be seen between the BBU growth data of Figure 4 and the transported current data of Figure 5.

Theoretical research[9] by Colombant and Lau predicts that the growth rate for the beam breakup instability can be reduced by up to a factor of two, depending upon the coupling strength. The physical mechanism for coupled cavity reduction of beam-breakup-instability growth is believed to be TM_{110} mode energy-sharing between internal and external cavities.

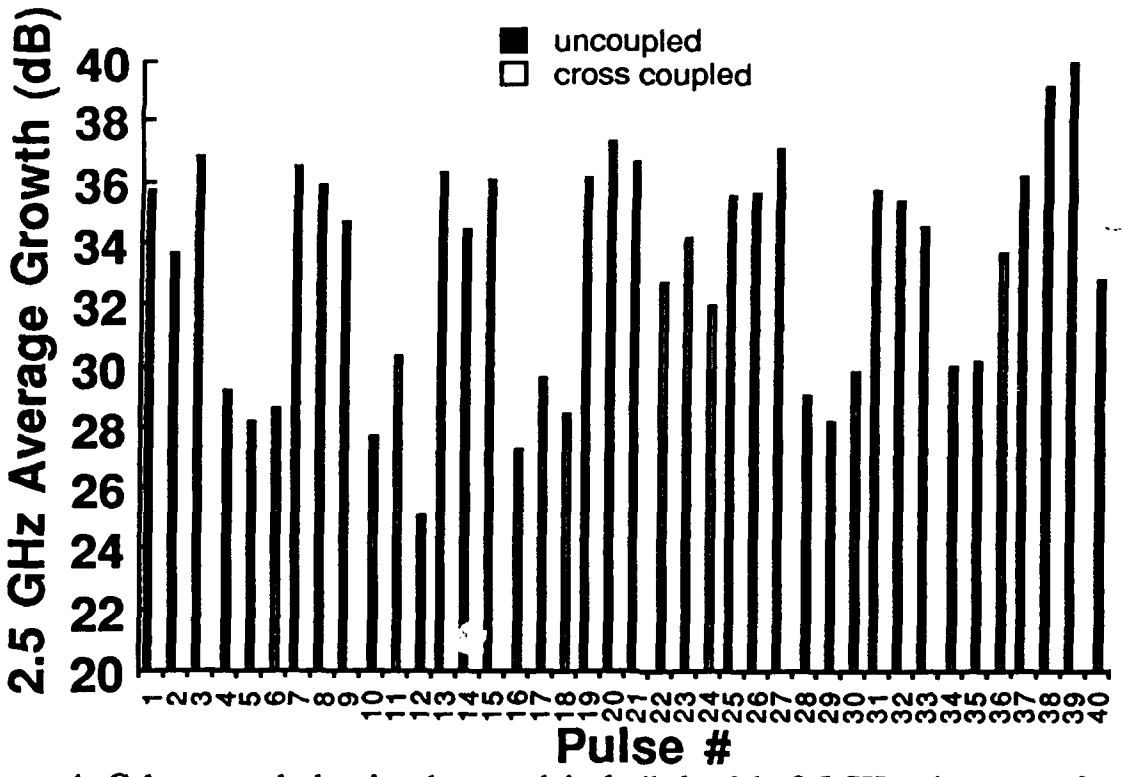

Figure 4. Column graph showing the growth in decibels of the 2.5 GHz microwaves for electron beam pulses in which the cavities were uncoupled (black columns) or cross coupled (open columns).

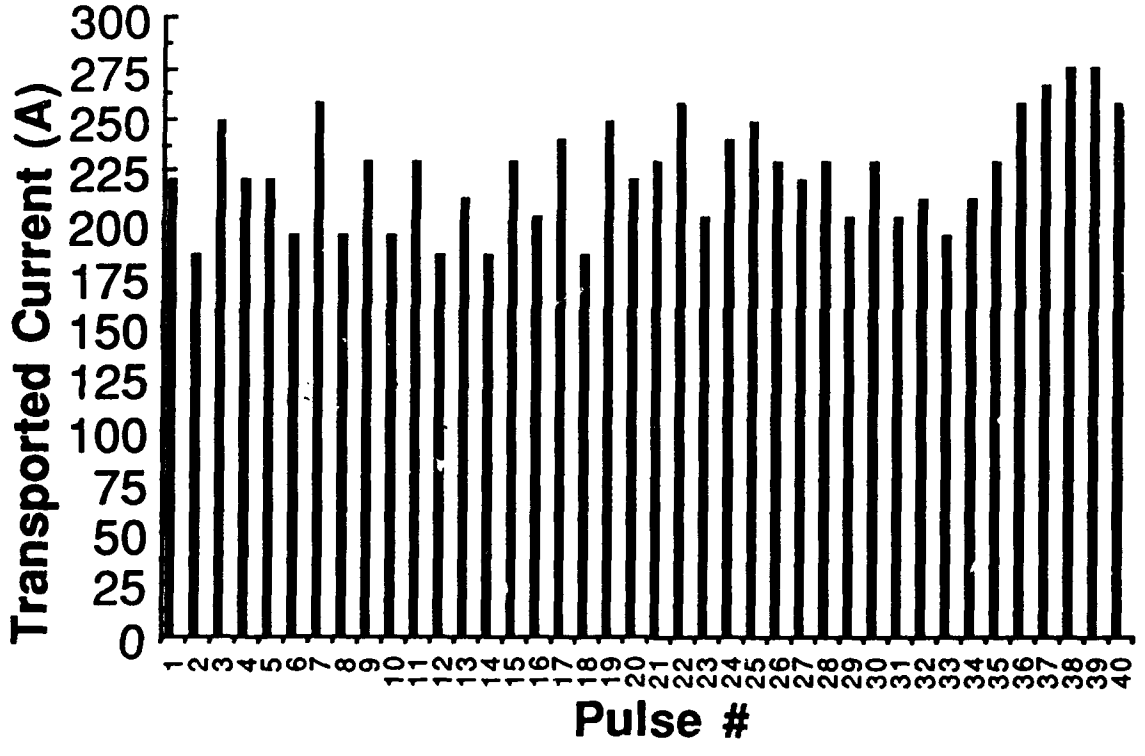

Figure 5. Column graph showing the amount of transported current for each electron beam pulse.

Acknowledgement

We appreciate valuable interactions with Y. Y. Lau. This research was supported by SDIO-IST through an ONR contract.

References

1) W. K. Panofsky and M. Bander, Rev. Sci. Instrum. **39**, 206 (1968)
2) Y. Y. Lau, Phys. Rev. Lett. **63** 1141 (1989)
3) K. Neil and R. K. Cooper, Part. Accel. **1**, 111 (1970)
4) K. Neil, L. S. Hall, and R. K. Cooper, Part. Accel. **9**, 213 (1970)
5) R. A. Bosch, P. R. Menge, and R. M. Gilgenbach, J. Appl. Phys. **71** 3091 (1992)
6) R. M. Gilgenbach, P. R. Menge, R. A. Bosch, J. J. Choi, C. H. Ching, and T.A Spencer, Conference Record of the 1991 Particle Accelerator Conference, IEEE Cat. No. 91CH3038-7
7) P.R. Menge, R. M. Gilgenbach, R.A. Bosch, C.H. Ching, T.A. Spencer, and M. Walter, in Intense Microwave and Particle Beams III, edited by H. Brandt, SPIE Vol. 1629, p 529, (1992)
8) D.G. Colombant, Y.Y. Lau, and D. Chernin, Part. Accel. **35** no. 4 Vol. 2, (1991)
9) D. G. Colombant and Y. Y. Lau, in Intense Microwave and Particle Beams III, edited by H. Brandt, SPIE Vol. 1629, p 538, (1992)
10) R. M. Gilgenbach, et al., in Digest of the 5th IEEE Pulsed Power Conference, p126 (IEEE, New York, NY, 1985)

The beam breakup instability in quadrupole and solenoidal electron-beam transport systems

R. A. Bosch,[a] P. R. Menge, and R. M. Gilgenbach
Intense Energy Beam Interaction Laboratory, Nuclear Engineering Department, The University of Michigan, Ann Arbor, Michigan 48109-2104

(Received 27 August 1991; accepted for publication 19 December 1991)

Dispersion relations are derived to determine the growth rate, dominant wavelength, and group velocity of disturbances caused by the beam breakup instability. Considerations include weak and strong focusing, x-y coupling in solenoidal transport, the spacing of accelerator cavities, and periodically pulsed beams. Beam breakup growth is minimum when the cavity spacing equals an integral number of half-betatron wavelengths for quadrupole focusing, and an integral number of betatron wavelengths for solenoidal focusing. Minimum growth is also found for periodic pulses separated by an integral number of half-periods of the TM_{110} cavity mode. Expressions for beam breakup growth at the minima are obtained.

I. INTRODUCTION

The acceleration and transport of high-brightness electron and ion beams are subject to disruption by the beam breakup (BBU) instability.[1-7] This instability results from coupling of transverse beam oscillations and a nonaxially symmetric mode of the accelerating structure. With cylindrical pillbox accelerating cavities, the TM_{110} mode produces the maximum instability growth.

In the regenerative BBU instability, upstream propagation of the TM_{110} mode provides feedback for amplification within a single accelerator section.[2] In the cumulative, or multisection, BBU instability, the TM_{110} modes of different accelerator sections are coupled only by the passage of the electron (or ion) beam. In this article, we study the cumulative BBU instability in linear focusing systems. In quadrupole focusing systems or systems containing certain nonaxisymmetric optical elements (e.g., magnetic sector field and edge focusing), the x and y directions of motion are not coupled.[8] With solenoidal transport, the BBU instability is affected by the coupling of the x and y directions of transverse motion.[9]

Our approach is to examine the BBU dispersion relations. This is a practical approach motivated by ongoing experiments:[10,11] the wavelength, e folding length, and group velocity of a BBU disturbance are directly obtainable from the dispersion relation. The dispersion relation may also be used in a study of the response to initial conditions, and calculation of beam offset versus time at a fixed position.[7]

We first consider continuum models of quadrupole and solenoidal transport, applicable when the accelerating cavity spacing is small compared to beam breakup scale lengths and the beam current is constant. Our results agree with several prior calculations.

We then consider the case of finite accelerator cavity spacing, treating the cavity forces as periodic impulses. For cavity spacing that is an integral number of half-betatron wavelengths with quadrupole transport, or an integral number of betatron wavelengths with solenoidal transport, BBU growth vanishes. When the finite cavity length is considered, BBU growth for these cavity spacings is calculated and found to be finite.

Finally, we consider the case of a pulsed beam. For pulses of vanishing pulse length separated by an integral multiple of one-half the TM_{110} period of the accelerating cavities, BBU growth vanishes. When a finite pulse length is considered, BBU growth no longer vanishes completely at these pulse separations. An expression for BBU growth with finite pulse length is presented.

II. THE ONE-DIMENSIONAL CONTINUUM MODEL FOR QUADRUPOLE TRANSPORT

We consider a beam transport system with periodically spaced cylindrical pillbox accelerating cavities. Transverse motions in the x and y directions are not coupled with quadrupole transport. Beam displacements in the x direction excite one polarization of the TM_{110} wavemode in the accelerator cavities, producing a magnetic field in the y direction on axis. The resultant $\mathbf{v}\times\mathbf{B}$ force is in the x direction. Consequently, the x and y directions of motion are not coupled in the BBU instability.

For quadrupole transport, the BBU instability has been studied previously using a one (transverse) -dimensional coupled-mode description.[3,7] The one-dimensional coupled-mode equations are

$$\frac{d}{dt}\gamma\frac{dx}{dt}+\gamma\omega_c^2 x=a, \tag{1a}$$

$$\left(\frac{\partial^2}{\partial t^2}+\frac{\omega_0}{Q}\frac{\partial}{\partial t}+\omega_0^2\right)a=2\gamma\omega_0^4\epsilon x, \tag{1b}$$

where $\gamma=(1-\beta^2)^{-1/2}$ is the relativistic mass factor, ω_c is the betatron angular frequency, and $d/dt=\partial/\partial t+v\partial/\partial z$ is the convective derivative. Equation (1a) describes the acceleration of the beam by the focusing field and the magnetic field B_y of the TM_{110} mode. Equation (1b) describes excitation of the TM_{110} mode with angular frequency ω_0

[a] Present address: Synchrotron Radiation Research Center, Hsinchu Science-based Industrial Park, Hsinchu, Taiwan, Republic of China.

 0021-8979/92/073091-12$04.00 © 1992 American Institute of Physics

C-1

($\omega_0 > 0$) and quality factor Q by the transverse beam disturbance. The quantity ϵ is the dimensionless coupling constant of the e beam to the TM_{110} mode, given by[12]

$$\epsilon = 0.422 \frac{l}{L} \frac{I}{17kA} \frac{\beta}{\gamma}, \tag{2a}$$

where l is the length of the microwave cavities, L is their spacing, and I is the beam current magnitude ($I > 0$). The coupling constant is related to the transverse impedance of Ref. 4 by

$$\epsilon = \frac{c}{60\omega_0 L} \frac{Z_\perp(\text{ohms})}{Q} \frac{I}{17kA} \frac{\beta}{\gamma}. \tag{2b}$$

For a coasting beam, v, γ, and ϵ are constant. Assuming a disturbance of the form $e^{i\omega t - ikz}$, Eqs. (1) and (2) yield the dispersion relation

$$\Omega^2 - \omega_c^2 + \Gamma = 0, \tag{3}$$

where

$$\Omega = \omega - vk \quad \text{and} \quad \Gamma = \frac{2\omega_0^4 \epsilon}{-\omega^2 + \omega_0^2 + i\omega\omega_0/Q}.$$

For real, positive values of ω, the magnitude of Γ is maximum for $\omega \cong \omega_0$, where $\Gamma(\omega_0) = -2i\omega_0^2 \epsilon Q$.

Scaling laws can be determined from the dispersion relation by considering the case where ω is real and positive. The e folding length of the instability is given by

$$l_e = [\mathrm{Im}(k)|_{\omega_{\max}}]^{-1}, \tag{4}$$

where $\omega_{\max}$ is the frequency giving the largest value of $\mathrm{Im}(k)$. In this model of the BBU instability, $\omega_{\max} \cong \omega_0$, with $\omega_0 (1 - 1/2\sqrt{3}Q) < \omega_{\max} < \omega_0$. The wavelength of maximum growth is

$$\lambda = \frac{2\pi}{Re(k)|_{\omega_{\max}}}. \tag{5}$$

The group velocity of a BBU disturbance dominated by the frequency $\omega_{\max}$ is given by

$$v_g = \left[\mathrm{Re}\left(\frac{\partial k}{\partial \omega} \right)\Big|_{\omega_{\max}} \right]^{-1} = \left(\frac{\partial k}{\partial \omega}\Big|_{\omega_{\max}} \right)^{-1}. \tag{6}$$

Consider a disturbance excited at $(z,t) = (0,0)$ and dominated by frequency $\omega_{\max}$. The time $t_{\max}$, at which the disturbance peaks at fixed z, is related to z by $t_{\max} = z/v_g$, while the disturbance amplitude grows as $e^{z/l_e} = e^{\mathrm{Im}(k)z}$.

For sufficiently weak focusing that $|\Gamma(\omega_0)| = 2\omega_0^2 \epsilon Q \gg \omega_c^2$, the dispersion relation reduces to

$$\Omega^2 + \Gamma = 0. \tag{7}$$

For $Q \gg 1$, maximum growth occurs for $\omega_{\max} = \omega_0 [1 - (1/2\sqrt{3}Q)]$, for which

$$k|_{\omega_{\max}} = \frac{1}{v}\left[\omega_0 \left(1 - \frac{1}{2\sqrt{3}Q} \right) \pm \omega_0 \epsilon^{1/2} Q^{1/2} \frac{3^{3/4}}{2} (i + 3^{-1/2}) \right], \tag{8}$$

$$\frac{\partial k}{\partial \omega}\Big|_{\omega_{\max}} = \frac{1}{v}\left(1 \pm \epsilon^{1/2} Q^{3/2} \frac{3^{3/4}}{2} \right). \tag{9}$$

The mode with $\mathrm{Im}(k) > 0$ propagates downstream as it grows.

For sufficiently strong focusing that $|\Gamma(\omega_0)| \ll \omega_c^2$, the e folding length given by Eq. (8) exceeds the betatron wavelength. In this strong focusing regime, the dispersion relation reduces to

$$\Omega = \pm(\omega_c^2 - \Gamma)^{1/2} \cong \pm[\omega_c - (\Gamma/2\omega_c)]. \tag{10}$$

Maximum instability growth is obtained at $\omega_{\max} = \omega_0$, for which

$$k|_{\omega_{\max}} = \frac{1}{v}\left[\omega_0 \pm \left(\omega_c + \frac{i\omega_0^2 \epsilon Q}{\omega_c} \right) \right], \tag{11}$$

$$\frac{\partial k}{\partial \omega}\Big|_{\omega_{\max}} = \frac{1}{v}\left(1 \pm 2\epsilon Q^2 \frac{\omega_0}{\omega_c} \right). \tag{12}$$

Because $\mathrm{Im}(k) \propto \epsilon \propto 1/L$, the growth per cavity in the strong focusing regime is independent of the cavity spacing. For weak and strong focusing, the e folding lengths and group velocities obtained from Eqs. (8), (9), (11), and (12) agree with asymptotic calculations of the response to an impulse[7] [see Eq. (12a) for weak focusing and Eq. (12b) for strong focusing in Ref. 7]. In the strong focusing regime, these results are also in agreement with the approach of Ref. 4, if a transfer matrix for quadrupole transport is employed.

III. A TWO-DIMENSIONAL CONTINUUM MODEL FOR SOLENOIDAL TRANSPORT

In solenoidal transport systems, transverse motions in the x and y directions are coupled by the $\mathbf{v} \times \mathbf{B}$ force. To model this case, we consider a two (transverse) -dimensional continuum description of the beam motion,[9]

$$\frac{d}{dt}\gamma \frac{dx}{dt} + \gamma\omega_c \frac{dy}{dt} = a_x, \tag{13a}$$

$$\frac{d}{dt}\gamma \frac{dy}{dt} - \gamma\omega_c \frac{dx}{dt} = a_y, \tag{13b}$$

where $\omega_c = eB/m\gamma$ is the relativistic cyclotron frequency. The TM_{110} modes of cylindrical pillbox accelerating cavities are excited by e-beam displacements according to

$$\left(\frac{\partial^2}{\partial t^2} + \frac{\omega_0}{Q}\frac{\partial}{\partial t} + \omega_0^2 \right) a_x = 2\gamma\omega_0^4 \epsilon x, \tag{14a}$$

$$\left(\frac{\partial^2}{\partial t^2} + \frac{\omega_0}{Q}\frac{\partial}{\partial t} + \omega_0^2 \right) a_y = 2\gamma\omega_0^4 \epsilon y. \tag{14b}$$

Equations (13) and (14) yield the dispersion relation

$$(\Omega^2 - \omega_c\Omega + \Gamma)(\Omega^2 + \omega_c\Omega + \Gamma) = 0. \tag{15}$$

While Eq. (15) is easily obtained directly from Eqs. (13) and (14), an alternative approach is to consider the helical Larmor frame: $x' = x\cos\theta + y\sin\theta$, $y' = y\cos\theta - x\sin\theta$, where $\theta = \omega_c z/2v$. This frame twists at one-

C-2

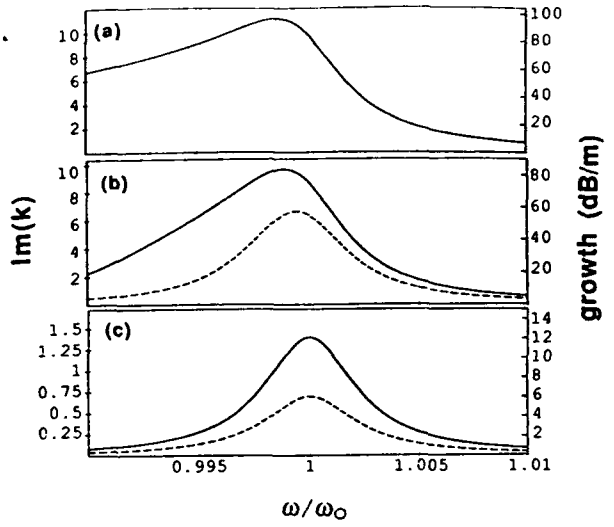

FIG. 1. The spatial growth rate $\mathrm{Im}(k)$ is graphed as a function of normalized angular frequency ω/ω_0, of the beam breakup wave. Curves are shown for the one-dimensional continuum model (dashed line) and the two-dimensional continuum model (solid line). The parameters used are kinetic energy = 700 keV, current = 100 A, TM_{110} mode frequency = 2.5 GHz, $Q = 200$, and $l/L = 0.15$. (a) Growth rates in the weak focusing regime, with a betatron wavelength of 5 m, and $|\Gamma(\omega_0)|/\omega_c^2 = 100$. In the weak focusing regime both models coincide, and the two curves lie atop each other. Note that the growth rate peaks at $\omega = \omega_{\max} = \omega_0[1 - (1/2\sqrt{3}Q)]$. (b) Growth rates for a case intermediate to the weak and strong focusing regimes, with a betatron wavelength of 0.5 m, and $|\Gamma(\omega_0)|/\omega_c^2 = 1$. (c) Growth rates in the strong focusing regime, with a betatron wavelength of 5 cm, and $|\Gamma(\omega_0)|/\omega_c^2 = 0.01$. Note that the growth rate peaks at $\omega = \omega_{\max} = \omega_0$.

half the rate of electron trajectories. In this frame, Eqs. (13) separate into two equations identical to Eq. (1a) with $\omega_c \to \omega_c/2$. Because the coordinate transformation is not time dependent, Eqs. (14) also hold in the helical frame. Consequently, the quadrupole focusing dispersion relation with $\omega_c \to \omega_c/2$ describes solenoidal focusing in the helical frame. Letting $\Omega \to \Omega - \omega_c/2$ or $\Omega \to \Omega + \omega_c/2$ (i.e., $k \to k \pm \omega_c/2v$) gives the corresponding laboratory frame dispersion relation.

For weak focusing with $|\Gamma(\omega_0)| \gg \omega_c^2$, Eq. (15) reduces to the one-dimensional results of Eq. (7). For strong focusing with $|\Gamma(\omega_0)| \ll \omega_c^2$, Eq. (15) reduces to

$$\Omega = \pm[\omega_c - (\Gamma/\omega_c)], \tag{16}$$

$$\Omega = \pm(\Gamma/\omega_c). \tag{17}$$

Comparing with Eq. (11), we find that a strong solenoidal focusing system with cylindrical pillbox cavities has twice the BBU growth of a quadrupole focusing system with the same betatron wavelength.

The e folding length and group velocity in the strong focusing regime are in agreement with Ref. 4. In a previous article,[9] we incorrectly stated that our results disagreed with Ref. 4 by a factor of 2, as a result of incorrectly relating the coupling constant ϵ to the transverse impedance. The correct relation is given by Eq. (2b).

In Fig. 1, we plot the growth rate versus ω for the one- and two-dimensional models [Eqs. (3) and (15)]. The growth rate is plotted in units of dB/m, where growth (dB/m) $= (20\log_{10}e)\mathrm{Im}(k)$ (m^{-1}). Figure 1(a) describes the weak focusing regime with $|\Gamma(\omega_0)|/\omega_c^2 = 100$. The two models give nearly identical results, and the peak growth occurs at $\omega_{\max} = \omega_0[1 - (1/2\sqrt{3}Q)]$. For the parameters used in Fig. 1(b), $|\Gamma(\omega_0)|/\omega_c^2 = 1.0$, so that the system is intermediate between the weak and strong focusing regimes. Figure 1(c) describes the strong focusing regime, with $|\Gamma(\omega_0)|/\omega_c^2 = 0.01$, in which solenoidal transport gives twice as much growth as quadrupole transport for the same value of ω_c, and BBU growth is largest at $\omega_{\max} = \omega_0$.

In actual accelerating cavities, the normally degenerate TM_{110} modes may be split because of perturbations to cylindrical symmetry from coupling loops, damping, slots, drive rods, etc.[2,13] We can model the case where the perturbed modes have vertical and horizontal polarizations by using separate resonant frequencies (ω_x and ω_y) and quality factors (Q_x and Q_y) for the linearly polarized modes in Equations (14a) and (14b).

For a disturbance of the form $e^{i\omega t - ikz}$, Eqs. (13) and (14) then yield the dispersion relation

$$\Omega^4 + \Omega^2(-\omega_c^2 + \Gamma_x + \Gamma_y) + \Gamma_x\Gamma_y = 0, \tag{18}$$

where $\Omega = \omega - kv$, $\Gamma_x = 2\omega_x^4\epsilon/(-\omega^2 + \omega_x^2 + i\omega\omega_x/Q)$, and $\Gamma_y = 2\omega_y^4\epsilon/(-\omega^2 + \omega_y^2 + i\omega\omega_y/Q)$. Note that Γ_x is a function of ω whose magnitude is maximum for $\omega \cong \omega_x$, while the magnitude of Γ_y is maximum for $\omega \cong \omega_y$.

In the weak focusing regime where $|\Gamma_x(\omega_x)|$, $|\Gamma_y(\omega_y)| \gg \omega_c^2$, Eq. (18) has solutions obeying $\Omega^2 + \Gamma_x = 0$ for $\omega \cong \omega_x$, and $\Omega^2 + \Gamma_y = 0$ for $\omega \cong \omega_y$. These results are identical to the one-dimensional result of Eq. (7).

In the strong focusing regime, $|\Gamma_x(\omega_x)|$, $|\Gamma_y(\omega_y)| \ll \omega_c^2$, the dispersion relation (18) becomes

$$\Omega = \pm\{\omega_c - [(\Gamma_x + \Gamma_y)/2\omega_c]\}, \tag{19}$$

$$\Omega = \pm(\Gamma_x\Gamma_y)^{1/2}/\omega_c. \tag{20}$$

If the TM_{110} modes have sufficiently different frequencies so that $|\omega_x - \omega_y| \gg \omega_x/Q_x, \omega_y/Q_y$, then Eqs. (19) and (20) are no longer approximated by Eqs. (16) and (17). A maximum in growth occurs for $\omega = \omega_x$, where Eq. (19) becomes $\Omega = \pm[\omega_c - \Gamma_x(\omega_x)/2\omega_c]$. Similarly, a maximum occurs for $\omega = \omega_y$, where Eq. (19) becomes $\Omega = \pm[\omega_c - \Gamma_y(\omega_y)/2\omega_c]$. These are identical to the results of the one-dimensional model. The growing mode of Eq. (20) has greatly reduced growth compared with Eq. (19).

In the strong focusing regime, a solenoidal focusing system with cylindrical pillbox cavities will have twice the BBU growth rate of a quadrupole focusing system with the same betatron wavelength. The solenoidal focusing growth rate may be halved by perturbing the cavities so that vertical and horizontal linear polarizations of the TM_{110} mode have sufficiently different resonant frequencies. However, if the perturbed cavities are oriented so that the linearly po-

larized modes of identical resonant frequency are aligned in the helical Larmor frame, BBU growth is not reduced by the perturbation.

The preceding equations treat the beam current as constant, and the transverse impulsive forces from the accelerating cavities as a continuous force per unit length. These approximations limit the dispersion relations to the cases where instability scale lengths (e folding length, wavelength) are long compared to the cavity spacing, and the beam current is constant.

IV. DISCRETE SPATIAL EFFECTS

A. One-dimensional model

If the betatron wavelength or BBU e folding length do not greatly exceed the spacing L of the accelerator cavities, we can no longer treat the transverse impulsive forces from the cavities as a continuous force per unit length. We consider a quadrupole focusing system with cavities of length l and separation L, with $l \ll L$. Treating the forces from the cavities as impulses, we have

$$\frac{d}{dt}\gamma\frac{dx}{dt}+\gamma\omega_c^2 x = aL\sum_{j=-\infty}^{\infty}\delta(z-jL), \tag{21}$$

$$\left(\frac{\partial^2}{\partial t^2}+\frac{\omega_0}{Q}\frac{\partial}{\partial t}+\omega_0^2\right)a = 2\gamma\omega_0^4\epsilon x. \tag{22}$$

These equations are invariant under space translation by distance L and arbitrary time translations. Thus, we consider solutions of the form $x = x_0(z)\,e^{i\omega t}$, where $x_0(z) = u(z)e^{-ikz}$, and $u(z)$ is periodic with period L. Because $e^{-ikL} = e^{-iL(k+2m\pi/L)}$ for integral values of m, k and $k + 2m\pi/L$ describe the same solution for any given ω. As a result, Ω and $\Omega - 2m\pi v/L$ describe the same solution for any given ω. Inserting the solution form, we obtain

$$\left[\left(i\omega+v\frac{d}{dz}\right)^2+\omega_c^2\right]x_0 = \Gamma x_0 L\sum_{j=-\infty}^{\infty}\delta(z-jL). \tag{23}$$

Because of the periodicity of $u(z)$, we need only solve Eq. (23) for $0<z<L$. In this region, the right-hand side of Eq. (23) vanishes, yielding the solution

$$x_0(z) = A\exp\left(\frac{iz}{v}(-\omega+\omega_c)\right) + B\exp\left(\frac{iz}{v}(-\omega-\omega_c)\right). \tag{24}$$

Continuity at $z=0$ implies

$$x_0(0+) = x_0(0-) = e^{ikL}x_0(L-), \tag{25}$$

while Eq. (23) implies the jump condition:

$$\frac{dx_0}{dz}(0+)-\frac{dx_0}{dz}(0-) = \frac{\Gamma L}{v^2}x_0(0), \tag{26}$$

where

$$\frac{dx_0}{dz}(0-) = e^{ikL}\frac{dx_0}{dz}(L-).$$

Inserting the ansatz (24) into Eqs. (25) and (26) yields two equations in three unknowns: A,B, and k. Eliminating A and B gives the dispersion relation

$$\cos\left(\frac{L\Omega}{v}\right) = \cos\frac{L\omega_c}{v}+\frac{\Gamma L}{2\omega_c v}\sin\frac{L\omega_c}{v}, \tag{27a}$$

where $\Omega = \omega - kv$. In the limit that the betatron wavelength and BBU e folding length are long compared with the cavity spacing, this equation reduces to the continuum dispersion relation of Eq. (3).

Equation (27a) may also be written as[14]

$$\left(-\omega^2+\omega_0^2+\frac{i\omega\omega_0}{Q}\right)\left(\cos\frac{L\Omega}{v}-\cos\frac{L\omega_c}{v}\right) = \frac{\omega_0^4\epsilon L}{\omega_c v}\sin\frac{L\omega_c}{v}. \tag{27b}$$

This form makes explicit the coupling between the cavity mode and the beam mode. For $kL = 2\pi n$ and complex ω, Eq. (27) gives the dispersion relation for a recirculating induction accelerator with one cavity, quadrupole focusing, and beam pulse length equal to the recirculation time.[15]

For $L = (n/2)\lambda_b$, where n is an integer and $\lambda_b = 2\pi v/\omega_c$ is the betatron wavelength, the dispersion relation becomes $\Omega = \pm\omega_c$. Thus, there is no BBU growth for any value of ω when the cavity spacing L equals $(n/2)\lambda_b$. Intuitively, this is a reasonable result: An impulse in the x direction provided by an accelerator cavity will not result in a deflection in the x direction in the subsequent cavity if the spacing is $(n/2)\lambda_b$, thwarting the mechanism of BBU growth. A finite level of BBU growth will result if the cavity spacing is not exactly equal to $(n/2)\lambda_b$ and because of the finite cavity length l.

In the strong focusing regime with $|\Gamma(\omega_0)| \ll \omega_c^2$, Eq. (27) is approximated by the one-dimensional continuum model dispersion relation of Eq. (10) for cavity spacings sufficiently far from $(n/2)\lambda_b$ that

$$|L-(n/2)\lambda_b|/L > |\Gamma(\omega_0)|/2\omega_c^2.$$

B. Two-dimensional model

For solenoidal focusing, a two-dimensional model can account for the discrete spatial effects when the cavity spacing L is not small compared to the betatron or BBU e folding length. We consider cylindrical pillbox cavities:

$$\frac{d}{dt}\gamma\frac{dx}{dt}+\gamma\omega_c\frac{dy}{dt} = a_x L\sum_{j=-\infty}^{\infty}\delta(z-jL), \tag{28a}$$

$$\frac{d}{dt}\gamma\frac{dy}{dt}-\gamma\omega_c\frac{dx}{dt} = a_y L\sum_{j=-\infty}^{\infty}\delta(z-jL), \tag{28b}$$

$$\left(\frac{\partial^2}{\partial t^2}+\frac{\omega_0}{Q}\frac{\partial}{\partial t}+\omega_0^2\right)a_x = 2\gamma\omega_0^4\epsilon x, \tag{29a}$$

$$\left(\frac{\partial^2}{\partial t^2}+\frac{\omega_0}{Q}\frac{\partial}{\partial t}+\omega_0^2\right)a_y = 2\gamma\omega_0^4\epsilon y. \tag{29b}$$

These equations are invariant under space translation by distance L and arbitrary time translations. Thus, we consider solutions of the form $x = x_0(z)\, e^{i\omega t}$, where $x_0(z) = u(z)e^{-ikz}$, and $u(z)$ is periodic with period L; and similarly for y. We thereby obtain

$$\left(i\omega + v\frac{d}{dz}\right)^2 x_0 + \omega_c\left(i\omega + v\frac{d}{dz}\right)y_0 = \Gamma x_0 L \sum_{j=-\infty}^{\infty} \delta(z - jL), \tag{30a}$$

$$\left(i\omega + v\frac{d}{dz}\right)^2 y_0 - \omega_c\left(i\omega + v\frac{d}{dz}\right)x_0 = \Gamma y_0 L \sum_{j=-\infty}^{\infty} \delta(z - jL). \tag{30b}$$

In the region $0<z<L$, the right-hand side of Eqs. (30) vanish, yielding the solution

$$x_0(z) = A\exp\left(\frac{iz}{v}(-\omega+\omega_c)\right) + B\exp\left(\frac{iz}{v}(-\omega-\omega_c)\right) + C\exp\left(\frac{-i\omega z}{v}\right), \tag{31a}$$

$$y_0(z) = -iA\exp\left(\frac{iz}{v}(-\omega+\omega_c)\right) + iB\exp\left(\frac{iz}{v}(-\omega-\omega_c)\right) - iD\exp\left(\frac{-i\omega z}{v}\right). \tag{31b}$$

Continuity at $z=0$ implies

$$x_0(0+) = x_0(0-) = e^{ikL}x_0(L-), \tag{32a}$$

$$y_0(0+) = y_0(0-) = e^{ikL}y_0(L-), \tag{32b}$$

while Eqs. (30) imply the jump conditions

$$\frac{dx_0}{dz}(0+) - \frac{dx_0}{dz}(0-) = \frac{\Gamma L}{v^2}x_0(0), \tag{33a}$$

$$\frac{dy_0}{dz}(0+) - \frac{dy_0}{dz}(0-) = \frac{\Gamma L}{v^2}y_0(0), \tag{33b}$$

where

$$\frac{dx_0}{dz}(0-) = e^{ikL}\frac{dx_0}{dz}(L-)$$

and

$$\frac{dy_0}{dz}(0-) = e^{ikL}\frac{dy_0}{dz}(L-).$$

Inserting the ansatz (31) into Eqs. (32) and (33) yields four equations in five unknowns: A,B,C,D, and k. Eliminating A,B,C, and D gives the dispersion relation

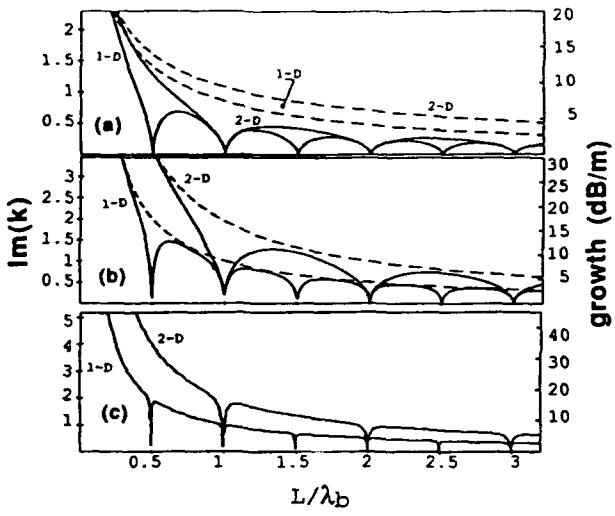

FIG. 2. Graphs of the spatial growth rate $\mathrm{Im}(k)$ as a function of the normalized cavity spacing L/λ_b. Dashed lines show the growth rates for the continuum models. Growth is shown at an angular frequency ω for which growth is near maximum. The parameters used are kinetic energy = 700 keV, current = 100 A, TM_{110} mode frequency = 2.5 GHz, Q = 200, and l = 1 cm. (a) Betatron wavelength = 5 m; $\omega = \omega_0[1 - (1/2\sqrt{3}Q)]$. (b) Betatron wavelength = 0.5 m; $\omega = \omega_0$. (c) Betatron wavelength = 5 cm; $\omega = \omega_0$.

$$\cos\left(\frac{L\Omega}{v} \pm \frac{L\omega_c}{2v}\right) = \cos\frac{L\omega_c}{2v} + \frac{\Gamma L}{\omega_c v}\sin\frac{L\omega_c}{2v}, \tag{34}$$

where $\Omega = \omega - kv$. Because Eqs. (28) and (29) are separable in the helical Larmor frame, Eq. (34) may also be obtained from Eq. (27a) by letting $\omega_c \to \omega_c/2$ and $\Omega \to \Omega \pm \omega_c/2$.

Four modes are described by Eq. (34). In the limit that the betatron wavelength and BBU e folding length are long compared with the cavity spacing, this equation reduces to the two-dimensional continuum dispersion relation of Eq. (15).

For $L = n\lambda_b$, where n is an integer, the dispersion relation becomes $\Omega = 0, \pm\omega_c$. Thus, there is no BBU growth for any value of ω when the cavity spacing L equals $n\lambda_b$, where λ_b is the betatron wavelength. Intuitively, this is a reasonable result: An impulse provided by an accelerator cavity will not result in a deflection in the subsequent cavity if the spacing is $n\lambda_b$, thwarting the mechanism of BBU growth. Unlike the one-dimensional model applicable to quadrupole focusing, a spacing of $(n/2)\lambda_b$, with odd integer n, will no longer suppress BBU growth. This is a result of x-y coupling. An impulse in the x direction will result in a deflection in the y direction in the subsequent cavity with a spacing of $(n/2)\lambda_b$ with odd integer n, so that the BBU instability can grow.

In the strong focusing regime, where $|\Gamma(\omega_0)| \ll \omega_c^2$, Eq. (34) is approximated by the two-dimensional continuum dispersion relations of Eqs. (16) and (17) for cavity spacings sufficiently far from $n\lambda_b$ that $|L - n\lambda_b|/L > 2|\Gamma(\omega_0)|/\omega_c^2$.

In Fig. 2, we display the BBU growth rate as a function of the normalized cavity spacing, L/λ_b, for the one-

and two-dimensional models that account for finite cavity spacing by treating cavity forces as impulses [Eqs. (27) and (34)]. The corresponding results from the continuum models [Eqs. (3) and (15)] are shown for comparison. In Fig. 2(a), the system is intermediate between the weak and strong focusing regimes; growth is significantly reduced by the finite cavity spacing, for the values of L/λ_b depicted. In Figs. 2(b) and 2(c), the systems are in the strong focusing regime. Finite cavity spacing reduces growth for $L/\lambda_b \cong n/2$ for the one-dimensional model, and $L/\lambda_b \cong n$ for the two-dimensional model, where n is an integer. As expected, the growth of the one-dimensional model is approximately equal to that predicted by the 1D continuum model for cavity spacings sufficiently different from $(n/2)\lambda_b$ that

$$|L-(n/2)\lambda_b|/L > |\Gamma(\omega_0)|/2\omega_c^2.$$

For the two-dimensional model, growth is approximated by the 2D continuum model for $|L - n\lambda_b|/L > 2|\Gamma(\omega_0)|/\omega_c^2$.

We finally consider the case where the linearly polarized TM_{110} modes that deflect in the x and y directions are perturbed so that their resonant frequencies are sufficiently different that $|\omega_x - \omega_y| > \omega_x/Q_x\omega_y/Q_y$. Then, for $\omega \cong \omega_x$, Eq. (30) approximately holds with $\Gamma = \Gamma_x$ on the right-hand side of Eq. (30a), and the right-hand side of Eq. (30b) set to zero. For a centered beam, Eq. (30b) can then be used to transform Eq. (30a) into the one-dimensional result of Eq. (23). Consequently, the one-dimensional dispersion relation of Eq. (27) will apply for $\omega \cong \omega_x$. Because this is an approximate result, the BBU growth for $L = (n/2)\lambda_b$ may not completely vanish. As in the continuum models, when the two linear polarizations of the TM_{110} mode are perturbed so that their frequency response curves do not greatly overlap, the one-dimensional dispersion relation applies.

C. Finite cavity length

The preceding calculations have shown that BBU growth vanishes with the proper choice of cavity spacing, if the forces from the cavities are modeled as impulses. We now consider the finite growth that will occur for nonzero cavity length l and errors in cavity spacing from an integral multiple of the half-betatron wavelength. We restrict the discussion to the one-dimensional model appropriate for quadrupole focusing. By letting $\omega_c \to \omega_c/2$ and $\Omega \to \Omega \pm \omega_c/2$, the dispersion relation we obtain will also be applicable to solenoidal focusing with cylindrically symmetric cavities.

For a cavity spacing $L = n\pi v/\omega_c + \delta$, where δ is the error in spacing from an integral multiple of the half-betatron wavelength, Eq. (27) gives the result for cavity forces modeled as impulses:

$$\Omega = \pm\omega_c \pm [-(\Gamma\delta/L)]^{1/2}. \tag{35}$$

Equation (35) is approximately true for $|\delta| \ll \lambda_b/2\pi$, where $\lambda_b = 2\pi v/\omega_c$ is the betatron wavelength. In addition, $|\Gamma\delta/L|^{1/2} \ll \omega_c/2\pi$ must be obeyed. Additional values for Ω differing by $2m\pi v/L$, where m is any integer, describe the same solution.

To model finite cavity lengths, we begin with the equations for finite cavity separation, replacing the δ function representing the impulsive acceleration in the cavity with a flattop function. This approach should be valid for small cavity lengths for which the electron transit time is small compared to the TM_{110} period. Thus, we have

$$\frac{d}{dt}\gamma\frac{dx}{dt} + \gamma\omega_c^2 x = aL\sum_{j=-\infty}^{\infty}\delta_l(z-jL), \tag{36}$$

$$\left(\frac{\partial^2}{\partial t^2} + \frac{\omega_0}{Q}\frac{\partial}{\partial t} + \omega_0^2\right)a = 2\gamma\omega_0^4\epsilon x. \tag{37}$$

Here, the function $\delta_l(z) = 1/l$ for $-l<z<0$ and zero elsewhere. These equations are invariant under space translation by distance L and arbitrary time translations, so we consider solutions of the form $x = x_0(z)\,e^{i\omega t}$, where $x_0(z) = u(z)e^{-ikz}$, and $u(z)$ is periodic with period L. We thereby obtain

$$\left[\left(i\omega + v\frac{d}{dz}\right)^2 + \omega_c^2\right]x_0 = \Gamma x_0 L\sum_{j=-\infty}^{\infty}\delta_l(z-jL). \tag{38}$$

Because of the periodicity of $u(z)$, we need only solve Eq. (38) for $-l<z<L-l$. In the region $0<z<L-l$, the right-hand side of Eq. (38) vanishes, yielding the solution

$$x_0(z) = A\exp\left(\frac{iz}{v}(-\omega+\omega_c)\right) + B\exp\left(\frac{iz}{v}(-\omega-\omega_c)\right). \tag{39}$$

For $-l<z<0$, we have

$$x_0(z) = C\exp\left\{\frac{iz}{v}\left[-\omega+\left(\omega_c^2-\frac{\Gamma L}{l}\right)^{1/2}\right]\right\} + D\exp\left\{\frac{iz}{v}\left[-\omega-\left(\omega_c^2-\frac{\Gamma L}{l}\right)^{1/2}\right]\right\}. \tag{40}$$

Continuity of x_0 implies that $x_0(0+) = x_0(0-)$ and

$$x_0(-l+) = x_0(-l-) = e^{ikL}x_0(L-l-).$$

Continuity of dx_0/dz at $z=-l$ and $z=0$ gives two analogous equations, so we have four equations in the unknowns A,B,C,D, and k. Eliminating A,B,C, and D, we have the equation

$$\begin{aligned}0 = {} & (M-P)(R-S)(e^{(P+M)L-(P+M)l} + e^{-2ikL-(P+M)l}) - (R-P)^2(e^{(P-ik)L-(P+R)l} \\ & + e^{(M-ik)L-(M+S)l}) + (S-P)^2(e^{(P-ik)L-(P+S)l} + e^{(M-ik)L-(M+R)l}),\end{aligned} \tag{41}$$

where $P = (i/v)(-\omega+\omega_c)$, $M = (i/v)(-\omega-\omega_c)$, $R = (i/v)[-\omega+(\omega_c^2-\Gamma L/l)^{1/2}]$, and $S = (i/v)[-\omega-(\omega_c^2-\Gamma L/l)^{1/2}]$.

Writing Eq. (41) in terms of $\Omega = \omega - vk$, ω_c, and $\theta = (\omega_c^2 - \Gamma L/l)^{1/2}$, we obtain a quadratic equation in $e^{iL\Omega/v}$, yielding the dispersion relation

$$\cos(L\Omega/v) = \alpha, \tag{42}$$

where

$$\alpha = -\frac{1}{4\omega_c\theta}\left[(\omega_c-\theta)^2\cos\left(\frac{\omega_c L}{v}-(\omega_c+\theta)\frac{l}{v}\right)\right.$$
$$\left.-(\omega_c+\theta)^2\cos\left(\frac{\omega_c L}{v}-(\omega_c-\theta)\frac{l}{v}\right)\right]. \quad (43)$$

If α is expanded to first order in l, Eq. (42) reduces to Eq. (27), where cavity forces are modeled as impulses. For cavity spacings close to an integral multiple of the half-betatron wavelength, $L = n\pi v/\omega_c + \delta$, where δ is the error in spacing. We expand Eq. (43) through fourth order in l and δ, noting that $\Gamma \propto \epsilon \propto l$, thereby obtaining the approximate dispersion relation

$$\Omega = \pm\omega_c\left(1-\frac{\delta}{L}\right)$$
$$\pm\left[-\frac{l\delta}{L^2}\left(\frac{\Gamma L}{l}\right)+\frac{\delta^2}{L^2}\omega_c^2\right.$$
$$+\frac{l^4}{L^4}\frac{n^2\pi^2}{12\omega_c^2}\left(\frac{\Gamma L}{l}\right)^2-\frac{l^3\delta}{L^4}\frac{n^2\pi^2}{6\omega_c^2}\left(\frac{\Gamma L}{l}\right)^2$$
$$\left.+\frac{l\delta^3}{L^4}\frac{n^2\pi^2}{6}\left(\frac{\Gamma L}{l}\right)-\frac{\delta^4}{L^4}\frac{n^2\pi^2\omega_c^2}{12}\right]^{1/2}. \quad (44)$$

The expression $(\Gamma L/l)$ has no dependence upon l. In order for Eq. (44) to be valid, it is necessary that $|\delta|, l \ll \lambda_b/2\pi$, and that the terms on the right-hand side containing δ and l be small compared to $\omega_c/n\pi$. We note that the lowest-order terms reproduce Eq. (35), where the forces from the cavities are modeled as impulses. For zero spacing error ($\delta = 0$), Eq. (44) becomes

$$\Omega = \pm\omega_c \pm \frac{l^2}{L^2}\frac{n\pi}{2\sqrt{3}\omega_c}\left(\frac{\Gamma L}{l}\right), \quad (45)$$

so that growth does not vanish for $L = (n/2)\lambda_b$ when finite cavity length is considered. Comparing Eqs. (35) and (45) in the strong focusing regime ($|\Gamma| \ll \omega_c^2$), we note that the BBU growth from a spacing error δ will exceed the growth from a cavity length l when $|\delta| \sim l$, unless n is very large. Thus, a spacing error will usually lead to greater BBU growth than a cavity length of comparable magnitude.

Comparing Eq. (45) with the continuum model dispersion relation in the strong focusing regime, Eq. (10), we note that BBU growth is modified by the factor $(2\pi/\sqrt{3}) \times (l/\lambda_b)$ when the cavity spacing is $(n/2)\lambda_b$. The reduction in BBU growth is substantial when $(l/\lambda_b) \ll 1$.

As an illustration of Eq. (45), we calculate the nonzero BBU growth resulting from the finite cavity length for quadrupole transport with $L = \lambda_b/2$, for the parameters of Fig. 2. For the parameters of Fig. 2(a), a cavity length of $l = 1$ cm gives $\mathrm{Im}(k) = 0.015\ \mathrm{m}^{-1}$, corresponding to a growth rate of 0.13 dB/m. For the case of Fig. 2(b), a growth of 1.3 dB/m is obtained. For the parameters of Fig. 2(c), a growth of 13 dB/m is given by Eq. (45). Because l/λ_b is not small compared to 1, the growth is not significantly reduced compared with the continuum model. Moreover, the requirement that $l \ll \lambda_b/2\pi$ is not obeyed for Fig. 2(c), so that 13 dB/m is not an accurate value.

V. PERIODICALLY PULSED BEAM

A. One-dimensional model

In this section, we consider a periodically pulsed beam, which can represent a micropulse train, in the limit of vanishing pulselength. The beam current is modeled as a train of δ functions separated by time τ. We assume that the betatron wavelength and BBU e folding length are long compared with the cavity separation, so that the impulsive transverse forces can be modeled as a continuous force per unit length. For a quadrupole focusing system, we have

$$\frac{d}{dt}\gamma\frac{dx}{dt}+\gamma\omega_c^2 x = a, \quad (46)$$

$$\left(\frac{\partial^2}{\partial t^2}+\frac{\omega_0}{Q}\frac{\partial}{\partial t}+\omega_0^2\right)a$$
$$= 2\gamma\omega_0^4\epsilon x\tau\sum_{j=-\infty}^{\infty}\delta\left[t-\left(j\tau+\frac{z}{v}\right)\right]. \quad (47)$$

The quantity ϵ is defined by Eq. (2) using the average beam current. Defining the variables $T = t - z/v$ and $Z = z$, we can write

$$v^2\gamma\frac{\partial^2 x}{\partial Z^2}+\gamma\omega_c^2 x = a, \quad (48)$$

$$\left(\frac{\partial^2}{\partial T^2}+\frac{\omega_0}{Q}\frac{\partial}{\partial T}+\omega_0^2\right)a = 2\gamma\omega_0^4\epsilon x\tau\sum_{j=-\infty}^{\infty}\delta(T-j\tau). \quad (49)$$

This system is invariant under arbitrary translations in Z, and periodic in T with period τ. We thus consider solutions of the form $a = a_0(T)e^{i\Omega Z/v}$ where $a_0(T) = u(T)e^{i\omega T}$, and $u(T)$ is periodic with period τ. In terms of the variables t and z, $a = u(t - z/v)e^{-ikz+i\omega t}$, where $\Omega = \omega - kv$. Because $e^{i\omega\tau} = e^{i\tau(\omega+2m\pi/\tau)}$ for integral m, ω, and $\omega + 2m\pi/\tau$ describe the same solution, giving the same value of Ω. Substituting the desired solution form into Eqs. (48) and (49) yields

$$\left(\frac{d^2}{dT^2}+\frac{\omega_0}{Q}\frac{d}{dT}+\omega_0^2\right)a_0 = \frac{2\omega_0^4\epsilon\tau a_0}{\omega_c^2-\Omega^2}\sum_{j=-\infty}^{\infty}\delta(T-j\tau). \quad (50)$$

In the region $0 < T < \tau$, the right-hand side of Eq. (50) vanishes, yielding the solution

$$a_0 = A\exp\{[i\omega_0\sqrt{1-(1/4Q^2)}-(\omega_0/2Q)]T\}$$
$$+B\exp\{[-i\omega_0\sqrt{1-(1/4Q^2)}$$
$$-(\omega_0/2Q)]T\}. \quad (51)$$

Continuity at $T = 0$ implies

C-7

$$a_0(0+) = a_0(0-) = e^{-i\omega\tau} a_0(\tau-), \tag{52}$$

while Eq. (50) implies the jump condition:

$$\frac{da_0}{dT}(0+) - \frac{da_0}{dT}(0-) = \frac{2\omega_0^4 \epsilon\tau a_0(0)}{\omega_c^2 - \Omega^2}, \tag{53}$$

where

$$\frac{da_0}{dT}(0-) = e^{-i\omega\tau} \frac{da_0}{dT}(\tau-).$$

Inserting the ansatz (51) into Eqs. (52) and (53) yields two equations in three unknowns: A,B, and Ω. Eliminating A and B gives the dispersion relation

$$\Omega^2 - \omega_c^2 = \frac{\omega_0^3 \epsilon\tau \sin[\omega_0\sqrt{1-(1/4Q^2)}\tau]}{2\sqrt{1-(1/4Q^2)}\sin\{[\omega_0\sqrt{1-(1/4Q^2)} - \omega + (i\omega_0/2Q)](\tau/2)\}\sin\{[-\omega_0\sqrt{1-(1/4Q^2)} - \omega + (i\omega_0/2Q)](\tau/2)\}}. \tag{54}$$

We note that ω and $\omega + 2m\pi/\tau$ give the same value of Ω, as expected. If the period between bunches τ is sufficiently small that $\omega_0\tau \ll 1$, and we consider frequencies ω sufficiently small that $\omega\tau \ll 1$, then the right-hand side of Eq. (54) reduces to $-\Gamma$, giving the one-dimensional continuum dispersion relation of Eq. (3). A BBU disturbance that does not oscillate in time is described by Eq. (54) with $\omega = 0$. Consequently, the growth rate given by Eq. (54) for $\omega = 0$ agrees with that obtained by other authors for a steady-state disturbance resulting from a misaligned beam[16,17] [see Eq. (47) of Ref. 16 and Eq. (16) of Ref. 17]. The growth rate given by Eq. (54) for $\omega_c = 0$ has also been described in Ref. 6.

We note that the right-hand side of Eq. (54) vanishes for $\tau = (n/2)\tau_0$, where $\tau_0 = 2\pi/(\omega_0\sqrt{1-1/4Q^2})$ is the period of the TM_{110} cavity mode. Thus, BBU growth vanishes when the bunch separation is an integral number of half-periods of the TM_{110} mode.[18]

For frequencies near ω_0, obeying $|\omega - \omega_0| \lesssim \omega_0/2Q$, and bunch separations sufficiently different from $(n/2)\tau_0$, obeying $|\tau - (n/2)\tau_0| \gg \tau/2Q$, and $n \ll Q$, the right-hand side of Eq. (54) reduces to $-\Gamma$, so that the one-dimensional continuum dispersion relation applies. Because $|\omega_{max} - \omega_0| \lesssim \omega_0/2Q$, BBU growth is given by the 1D continuum theory for $|\tau - (n/2)\tau_0| \gg \tau/2Q$ and $n \ll Q$.

B. TWO-DIMENSIONAL MODEL

For a periodically pulsed beam in a solenoidal focusing system with cylindrical pillbox cavities, we consider a two-dimensional model. Again, we assume that the betatron wavelength and BBU e folding length are long compared with the cavity separation so that a continuum description can be used for the acceleration of the beam by the cavities. In terms of the variables $T = t - z/v$ and $Z = z$, we have

$$v^2\gamma \frac{\partial^2 x}{\partial Z^2} + \gamma\omega_c v \frac{\partial y}{\partial Z} = a_x, \tag{55a}$$

$$v^2\gamma \frac{\partial^2 y}{\partial Z^2} - \gamma\omega_c v \frac{\partial x}{\partial Z} = a_y, \tag{55b}$$

$$\left(\frac{\partial^2}{\partial T^2} + \frac{\omega_0}{Q}\frac{\partial}{\partial T} + \omega_0^2\right) a_x = 2\gamma\omega_0^4 \epsilon x\tau \sum_{j=-\infty}^{\infty} \delta(T - j\tau), \tag{56a}$$

$$\left(\frac{\partial^2}{\partial T^2} + \frac{\omega_0}{Q}\frac{\partial}{\partial T} + \omega_0^2\right) a_y = 2\gamma\omega_0^4 \epsilon y\tau \sum_{j=-\infty}^{\infty} \delta(T - j\tau). \tag{56b}$$

This system is invariant under arbitrary translations in Z, and periodic in T with period τ. We thus consider solutions of the form $a_x = a_{x0}(T)e^{i\Omega Z/v}$ where $a_{x0}(T) = u(T)e^{i\omega T}$, and $u(T)$ is periodic with period τ. A similar form is assumed for a_y, x, and y. In terms of the variables t and z, $a_x = u(t - z/v)e^{-ikz + i\omega t}$, where $\Omega = \omega - kv$. Substituting this solution form into Eqs. (55) and (56) yields

$$\left(\frac{d^2}{dT^2} + \frac{\omega_0}{Q}\frac{d}{dT} + \omega_0^2\right) a_{x0} = \frac{2\omega_0^4 \epsilon\tau(a_{x0} + i\omega_c a_{y0}/\Omega)}{\omega_c^2 - \Omega^2} \sum_{j=-\infty}^{\infty} \delta(T - j\tau), \tag{57a}$$

$$\left(\frac{d^2}{dT^2} + \frac{\omega_0}{Q}\frac{d}{dT} + \omega_0^2\right) a_{y0} = \frac{2\omega_0^4 \epsilon\tau(a_{y0} - i\omega_c a_{x0}/\Omega)}{\omega_c^2 - \Omega^2} \sum_{j=-\infty}^{\infty} \delta(T - j\tau). \tag{57b}$$

In the region $0 < T < \tau$, the right-hand side of Eqs. (57) vanishes, yielding the solution

$$a_{x0} = A\exp\left\{\left[i\omega_0\left(1 - \frac{1}{4Q^2}\right)^{1/2} - \frac{\omega_0}{2Q}\right]T\right\} + B\exp\left\{\left[-i\omega_0\left(1 - \frac{1}{4Q^2}\right)^{1/2} - \frac{\omega_0}{2Q}\right]T\right\}, \tag{58a}$$

$$a_{y0} = C\exp\left\{\left[i\omega_0\left(1 - \frac{1}{4Q^2}\right)^{1/2} - \frac{\omega_0}{2Q}\right]T\right\} + D\exp\left\{\left[-i\omega_0\left(1 - \frac{1}{4Q^2}\right)^{1/2} - \frac{\omega_0}{2Q}\right]T\right\}. \tag{58b}$$

Continuity at $T = 0$ implies

$$a_{x0}(0+) = a_{x0}(0-) = e^{-i\omega\tau} a_{x0}(\tau-), \tag{59a}$$

$$a_{y0}(0+) = a_{y0}(0-) = e^{-i\omega\tau} a_{y0}(\tau-), \tag{59b}$$

while Eqs. (57) imply the jump conditions:

$$\frac{da_{x0}}{dT}(0+) - \frac{da_{x0}}{dT}(0-) = \frac{2\omega_0^4 \epsilon\tau [a_{x0}(0) + i\omega_c a_{y0}(0)/\Omega]}{\omega_c^2 - \Omega^2}, \tag{60a}$$

$$\frac{da_{y0}}{dT}(0+) - \frac{da_{y0}}{dT}(0-) = \frac{2\omega_0^4 \epsilon\tau [a_{y0}(0) - i\omega_c a_{x0}(0)/\Omega]}{\omega_c^2 - \Omega^2}, \tag{60b}$$

where

$$\frac{da_{x0}}{dT}(0-) = e^{-i\omega\tau} \frac{da_{x0}}{dT}(\tau-)$$

and

$$\frac{da_{y0}}{dT}(0-) = e^{-i\omega\tau} \frac{da_{y0}}{dT}(\tau-).$$

Inserting the ansatz (58) into Eqs. (59) and (60) yields four equations in five unknowns: A,B,C,D, and Ω. Eliminating A,B,C, and D gives the dispersion relation

$$\Omega^2 \pm \omega_c \Omega = \frac{\omega_0^3 \epsilon\tau \sin[\omega_0 \sqrt{1-(1/4Q^2)}\,\tau]}{2\sqrt{1-(1/4Q^2)}\sin\{[\omega_0\sqrt{1-(1/4Q^2)} - \omega + (i\omega_0/2Q)](\tau/2)\}\sin\{[-\omega_0\sqrt{1-(1/4Q^2)} - \omega + (i\omega_0/2Q)](\tau/2)\}}. \tag{61}$$

Equation (61) can also be obtained directly from Eq. (54) by letting $\omega_c \to \omega_c/2$ and $\Omega \to \Omega \pm \omega_c/2$. If the period between bunches τ is sufficiently small that $\omega_0\tau \ll 1$, and we consider frequencies ω sufficiently small that $\omega\tau \ll 1$, then the right-hand side of Eq. (61) reduces to $-\Gamma$, giving the two-dimensional continuum dispersion relation of Eq. (15). The right-hand side of Eq. (61) vanishes for

$$\tau = n\pi/(\omega_0\sqrt{1-1/4Q^2}) = (n/2)\tau_0.$$

Thus, BBU growth vanishes when the bunch separation is an integral number of half-periods of the TM_{110} mode, as in the case of quadrupole focusing.

For frequencies near ω_0, obeying $|\omega - \omega_0| \lesssim \omega_0/2Q$, and bunch separations sufficiently different from $(n/2)\tau_0$, obeying $|\tau - (n/2)\tau_0| \gg \tau/2Q$, and $n \ll Q$, the right-hand side of Eq. (61) reduces to $-\Gamma$, so that the two-dimensional continuum dispersion relation applies. Thus, for $|\tau - (n/2)\tau_0| \gg \tau/2Q$ and $n \ll Q$, BBU growth is given by the 2D continuum theory.

In Fig. 3, we plot the growth rate versus the normalized bunch separation for the one- and two-dimensional models [Eqs. (54) and (61)]. Figure 3(a) describes the weak focusing regime, Fig. 3(b) describes a case intermediate between the weak and strong focusing regimes, while Fig. 3(c) describes the strong focusing regime. As in the continuum case, nearly identical growth rates are obtained by the two models in the weak focusing regime, while the two-dimensional model gives twice the growth of the one-dimensional model in the strong focusing regime. BBU growth vanishes for $\tau = (n/2)\tau_0$, where n is an integer and $\tau_0 = 2\pi/(\omega_0\sqrt{1-1/4Q^2})$ is the period of the TM_{110} cavity mode with finite Q. In Figs. 3(a) and 3(b), growth is maximized for $\tau = (n/2)\tau_0(1 + 1/2Q)$, as in the case of a steady-state ($\omega = 0$) disturbance.[6,16] This maximum in growth is pronounced when Q is sufficiently large. For $|\tau - (n/2)\tau_0| \gg \tau/2Q$, BBU growth is the same as that calculated by the continuum models in Fig. 1, as expected.

Finally, we consider solenoidal focusing with perturbed cavities in which the vertical and horizontal polarizations of the TM_{110} mode have sufficiently different resonant frequencies so that, for $\omega \cong \omega_x$, the y polarization is

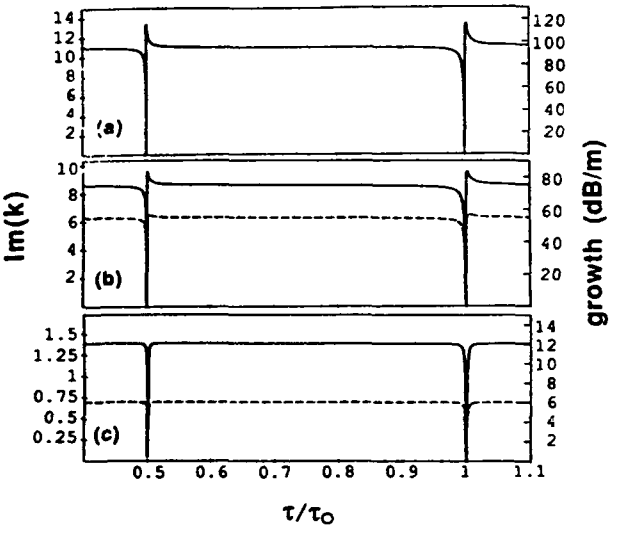

FIG. 3. Graphs of the spatial growth rate $\mathrm{Im}(k)$ as a function of the normalized bunch separation time τ/τ_0. Curves are shown for the one-dimensional model (dashed line) and the two-dimensional model (solid line). Growth is shown at an angular frequency ω for which growth is near maximum. The parameters used are: kinetic energy = 700 keV, current = 100 A, TM_{110} mode frequency = 2.5 GHz, $Q = 200$, and $l/L = 0.15$. (a) Growth rates in the weak focusing regime, with a betatron wavelength of 5 m, and $|\Gamma(\omega_0)|/\omega_c^2 = 100$; $\omega = \omega_0[1 - (1/2\sqrt{3}Q)]$. (b) Growth rates for a case intermediate between the weak and strong focusing regimes, with a betatron wavelength of 0.5 m, and $|\Gamma(\omega_0)|/\omega_c^2 = 1$; $\omega = \omega_0$. (c) Growth rates for a strong focusing case, with a betatron wavelength of 5 cm, and $|\Gamma(\omega_0)|/\omega_c^2 = 0.01$; $\omega = \omega_0$.

C-9

not excited. Then, the term a_{y0} vanishes in Eq. (60a), for $\omega \cong \omega_x$. Consequently, Eqs. (59a) and (60a) are the same as Eqs. (52) and (53) of the one-dimensional model. The one-dimensional dispersion relation of Eq. (54) will then apply for $\omega \cong \omega_x$.

C. Pulsed beam with finite pulse length

Recently, there has been interest in achieving low BBU growth by using a pulsed beam with bunch separation equal to an integral number of half-periods of the TM_{110} mode.[18] In this subsection, we consider the finite BBU growth that is expected from finite pulse lengths and bunch separations differing slightly from $(n/2)\tau_0$. We restrict the discussion to quadrupole focusing systems. By letting $\omega_c \to \omega_c/2$ and $\Omega \to \Omega \pm \omega_c/2$, the dispersion relations we obtain will also describe solenoidal focusing with cylindrical symmetry.

For the case of δ-function bunches whose bunch separation is $\tau = (n/2)\tau_0 + \delta$, where the timing error $|\delta| < \pi/(\omega_0\sqrt{1-1/4Q^2}) = \tau_0/2$, the dispersion relation of Eq. (54) reduces to

$$\Omega^2 - \omega_c^2 = \begin{cases} \dfrac{\omega_0^4 \epsilon \tau \delta}{2\sin^2\{[\omega - (i\omega_0/2Q)](\tau/2)\}}, & \text{for } n \text{ even}, \\ \dfrac{\omega_0^4 \epsilon \tau \delta}{2\cos^2\{[\omega - (i\omega_0/2Q)](\tau/2)\}}, & \text{for } n \text{ odd}. \end{cases} \tag{62}$$

This approximation is valid when $|\omega_0\delta| < n\pi/2Q$ and $|\omega_0\delta| \ll 1$.

We now calculate an analogous result for the BBU growth resulting from a finite pulse duration Δ, where th quantity Δ is in units of time. To model a finite pulse length, we consider the model of Eqs. (48) and (49), where the δ function on the right-hand side of Eq. (49) is replaced by a flattop function: $\delta_\Delta(T) = 1/\Delta$ for $-\Delta < T < 0$, and zero elsewhere:

$$v^2\gamma \frac{\partial^2 x}{\partial Z^2} + \gamma\omega_c^2 x = a, \tag{63}$$

$$\left(\frac{\partial^2}{\partial T^2} + \frac{\omega_0}{Q}\frac{\partial}{\partial T} + \omega_0^2\right)a = 2\gamma\omega_0^4 \epsilon x \tau \sum_{j=-\infty}^{\infty} \delta_\Delta(T - j\tau). \tag{64}$$

This system is invariant under arbitrary translations in Z, and periodic in T with period τ. We thus consider solutions of the form $a = a_0(T)e^{i\Omega Z/v}$ where $a_0(T) = u(T)e^{i\omega T}$, and $u(T)$ is periodic with period τ. Substituting this solution form into Eqs. (63) and (64) yields

$$\left(\frac{d^2}{dT^2} + \frac{\omega_0}{Q}\frac{d}{dT} + \omega_0^2\right)a_0 = \frac{2\omega_0^4 \epsilon \tau a_0}{\omega_c^2 - \Omega^2} \sum_{j=-\infty}^{\infty} \delta_\Delta(T - j\tau). \tag{65}$$

This equation can be solved in the region $0 < T < \tau - \Delta$ to give

$$a_0 = A\exp\left\{\left[i\omega_0\left(1 - \frac{1}{4Q^2}\right)^{1/2} - \frac{\omega_0}{2Q}\right]T\right\} + B\exp\left\{\left[-i\omega_0\left(1 - \frac{1}{4Q^2}\right)^{1/2} - \frac{\omega_0}{2Q}\right]T\right\}. \tag{66}$$

In the region $-\Delta < T < 0$, Eq. (65) is solved by

$$a_0 = C\exp\left[i\omega_0\left(1 - \frac{1}{4Q^2} - \frac{2\omega_0^2\epsilon\tau}{\Delta(\omega_c^2 - \Omega^2)}\right)^{1/2} - \frac{\omega_0}{2Q}\right]T + D\exp\left[-i\omega_0\left(1 - \frac{1}{4Q^2} - \frac{2\omega_0^2\epsilon\tau}{\Delta(\omega_c^2 - \Omega^2)}\right)^{1/2} - \frac{\omega_0}{2Q}\right]T. \tag{67}$$

At the times $T = 0$ and $T = -\Delta$, a_0 and da_0/dT are continuous. Using the relations $a_0(-\Delta-) = e^{-i\omega\tau}a_0(\tau-\Delta-)$ and

$$\frac{da_0}{dT}(-\Delta-) = e^{-i\omega\tau}\frac{da_0}{dT}(\tau-\Delta-),$$

we obtain four equations in the unknowns A,B,C,D, and Ω. Eliminating A,B,C, and D, we obtain the equation

$$\begin{aligned} 0 = {} & (M-P)(R-S)(e^{(P+M)\tau-(P+M)\Delta} + e^{2i\omega\tau-(P+M)\Delta}) - (R-P)^2(e^{(P+i\omega)\tau-(P+R)\Delta} \\ & + e^{(M+i\omega)\tau-(M+S)\Delta}) + (S-P)^2 \\ & \times (e^{(P+i\omega)\tau-(P+S)\Delta} + e^{(M+i\omega)\tau-(M+R)\Delta}), \end{aligned} \tag{68}$$

where

$$P = i\omega_0(1-1/4Q^2)^{1/2} - (\omega_0/2Q),$$

$$M = -i\omega_0(1-1/4Q^2)^{1/2} - (\omega_0/2Q),$$

$$R = i\omega_0\{1 - 1/4Q^2 - 2\omega_0^2\epsilon\tau/[\Delta(\omega_c^2-\Omega^2)]\}^{1/2} - (\omega_0/2Q),$$

and

$$S = -i\omega_0\{1 - 1/4Q^2 - 2\omega_0^2\epsilon\tau/[\Delta(\omega_c^2-\Omega^2)]\}^{1/2} - (\omega_0/2Q).$$

Defining the frequencies $\omega_1 = \omega_0(1 - 1/4Q^2)^{1/2}$ and $\omega_2 = \omega_0\{1 - 1/4Q^2 - 2\omega_0^2\epsilon\tau/[\Delta(\omega_c^2-\Omega^2)]\}^{1/2}$, Eq. (68) gives the dispersion relation

$$\begin{aligned} 0 = {} & 4\omega_1\omega_2\cos[\omega - (i\omega_0/2Q)]\tau \\ & + (\omega_1-\omega_2)^2\cos[\omega_1\tau - (\omega_1+\omega_2)\Delta] \\ & - (\omega_1+\omega_2)^2\cos[\omega_1\tau - (\omega_1-\omega_2)\Delta]. \end{aligned} \tag{69}$$

For a short pulse duration, $\Delta \ll \tau_0/2$, and bunch separation close to an integral number of half-cavity periods,

$$\tau = n\pi/(\omega_0\sqrt{1-1/4Q^2}) + \delta = (n/2)\tau_0 + \delta,$$

where $|\delta| \ll \tau_0$, the last two cosines in Eq. (69) can be expanded through fourth order to yield an approximate dispersion relation for the BBU instability:

$$\Omega^2 - \omega_c^2 = \frac{\omega_0^4 \epsilon \tau}{\xi}\left[-\delta \pm \left(\delta^2 + \frac{2\xi\delta\Delta}{3} - \frac{\xi\Delta^2}{3}\right)^{1/2}\right], \qquad (70)$$

where

$$\xi = -2(1-(-1)^n \cos\{[\omega - (i\omega_0/2Q)]\tau\}).$$

Equation (70) is approximately obeyed for sufficiently small timing errors and pulse lengths satisfying $|\omega_0\delta| \ll n\pi/2Q \ll 1/2\sqrt{3}$, and $|\omega_0\Delta| \ll 1$. Because $n\pi \cong \omega_0\tau$, the TM_{110} mode must not decay significantly between pulses. In addition, $|\xi| \ll 1$ is required, which is satisfied when $|\omega - \omega_0| \ll \omega_0/2n\pi\sqrt{3}$. This is not a severe restriction since frequencies near ω_0 give the greatest BBU growth and thus are of primary interest. For $\Delta = 0$ (vanishing pulselength), Eq. (70) gives the BBU dispersion relation of Eq. (62), as expected. In addition, the nongrowing roots $\Omega^2 - \omega_c^2 = 0$ occur. For $\delta = 0$ (no timing error), Eq. (70) becomes

$$\Omega^2 - \omega_c^2 = \begin{cases} \pm\dfrac{\omega_0^4 \epsilon\tau\Delta}{2\sqrt{3}\sin\{[\omega - (i\omega_0/2Q)](\tau/2)\}}, & \text{for } n \text{ even}, \\ \pm\dfrac{\omega_0^4 \epsilon\tau\Delta}{2\sqrt{3}\cos\{[\omega - (i\omega_0/2Q)](\tau/2)\}}, & \text{for } n \text{ odd}. \end{cases} \qquad (71)$$

Equation (71) shows that BBU growth occurs in the absence of a timing error because of the finite pulse duration of the electron bunches. Electron bunches of finite pulsewidth Δ can also be modeled by "head" and "tail" macroparticles rather than a flattop pulse.[18] In this approach, the flattop (δ_Δ) term in Eq. (64) is replaced by $[\delta(T - j\tau) + \delta(T - j\tau + \Delta)]/2$. For zero timing error, we obtain a dispersion relation identical to Eq. (71) with $\Delta \to \sqrt{3}\Delta$. Increased BBU growth results from the concentration of current at the head and tail of the pulse.

In the strong focusing regime, maximum growth occurs for $\omega \cong \omega_0$. At this frequency, Eq. (71) becomes

$$\Omega^2 - \omega_c^2 = \pm(2\pi/\sqrt{3})(\Delta/\tau_0)\Gamma(\omega_0). \qquad (72)$$

In comparison with the continuum model of Eq. (3), Γ is multiplied by the factor $(2\pi/\sqrt{3})$ (Δ/τ_0), so that BBU growth is modified by this factor for pulses separated by $(n/2)\tau_0$ in the strong focusing regime. Thus, for $(\Delta/\tau_0) \ll 1$, significant BBU growth reduction can be obtained by the use of a pulsed current.

In Fig. 4 we display the results of Eq. (70) for the parameters of Fig. 3 and two different nonzero pulse lengths. We also show the results of Eq. (54) for δ-function pulses. The finite pulse lengths result in nonzero BBU growth for all values of pulse spacing τ, and a shift in the value of τ that gives minimum BBU growth. With a finite pulse length, $\tau = (n/2)\tau_0$ no longer gives minimum BBU growth, so that a slight timing adjustment may be advantageous in applications using a pulsed beam.

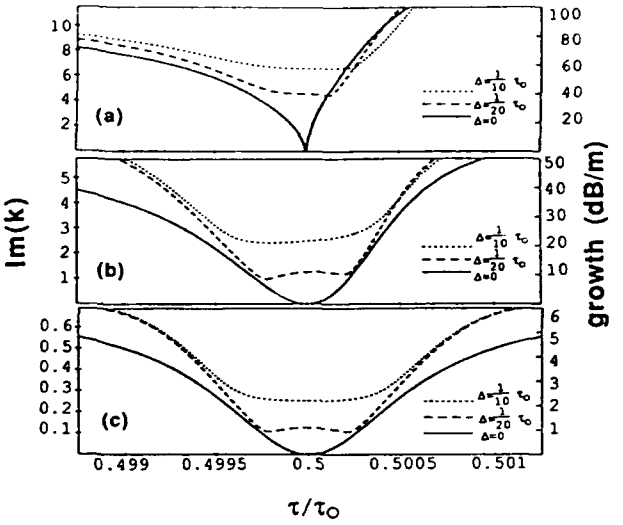

FIG. 4. Graphs of the spatial growth rate $\mathrm{Im}(k)$ as a function of normalized bunch separation time τ/τ_0 for different values of pulse length Δ. Growth is shown at an angular frequency ω for which growth is near maximum. Curves are shown for pulselengths of $\Delta = 0$ (solid black line), $\Delta = \frac{1}{20}\tau_0$ (dashed line), and $\Delta = \frac{1}{10}\tau_0$ (dotted line). The parameters used are: kinetic energy = 700 keV, current = 100 A, TM_{110} mode frequency = 2.5 GHz, $Q = 200$, and $l/L = 0.15$. (a) Growth rates in the weak focusing regime, with a betatron wavelength of 5 m, and $|\Gamma(\omega_0)|/\omega_c^2 = 100$; $\omega = \omega_0[1 - (1/2\sqrt{3}Q)]$. (b) Growth rates for a case intermediate between the weak and strong focusing regimes, with a betatron wavelength of 0.5 m, and $|\Gamma(\omega_0)|/\omega_c^2 = 1$; $\omega = \omega_0$. (c) Growth rates in the strong focusing regime, with a betatron wavelength of 5 cm, and $|\Gamma(\omega_0)|/\omega_c^2 = 0.01$; $\omega = \omega_0$.

VI. SUMMARY

Dispersion relations for the BBU instability have been derived for quadrupole and solenoidal focusing. We first considered a continuum model appropriate for constant beam current and cavity spacings small compared to the betatron wavelength and e folding length of BBU growth. The x-y coupling of solenoidal focusing affects the BBU growth rate for cylindrical pillbox accelerator cavities, in which the TM_{110} frequency is independent of polarization. BBU growth in the strong focusing regime is twice that of a quadrupole focusing system with the same betatron wavelength. By perturbing the cavities so that the vertical and horizontal polarizations of the TM_{110} mode have sufficiently different resonant frequencies, this growth may be halved.

A model was presented for the case where the spacing of the accelerator cavities can be large compared to the betatron wavelength and the e folding length of BBU growth. We first neglected the finite length of the cavities. For quadrupole focusing, BBU growth vanishes when the spacing is an integral multiple of one-half betatron wavelength. With solenoidal focusing and cylindrical pillbox cavities, the cavity spacing must be an integral multiple of the betatron wavelength to prevent BBU growth. Finally, we considered the effect of finite cavity length with quadrupole focusing, showing that the BBU growth does not completely vanish for spacings that are integral multiples of one-half betatron wavelength. For such spacings in the

strong focusing regime, BBU growth is modified by the factor $(2\pi/\sqrt{3})$ (l/λ_b) when compared to the continuum model, where l is the cavity length, λ_b is the betatron wavelength, and $(l/\lambda_b) \ll 1/2\pi$.

A model was also presented for a periodically pulsed electron-beam current. We first considered vanishing pulselength by modeling δ-function current pulses. BBU growth vanishes when the pulse separation is a multiple of one-half of the TM_{110} period, for both quadrupole and solenoidal focusing. When a finite pulselength was considered, the BBU growth did not completely vanish. For pulse separations that are a multiple of one-half of the TM_{110} period in the strong focusing regime, BBU growth is modified by the factor $(2\pi/\sqrt{3})$ (Δ/τ_0) when compared to the continuum model, where Δ is the pulse duration, τ_0 is the period of the TM_{110} mode, and $(\Delta/\tau_0) \ll 1/2\pi$.

Because the e folding length, wavelength, and group velocity of the BBU instability are directly calculable from the dispersion relation, the formulas presented here may be used to calculate these important quantities under a broad range of conditions.

ACKNOWLEDGMENTS

We appreciate valuable discussions with Y. Y. Lau. This research was supported by the Strategic Defense Initiative through an Office of Naval Research contract.

[1] W. K. H. Panofsky and M. Bander, Rev. Sci. Instrum. 39, 206 (1968).
[2] R. Helm and G. Loew, "Beam Breakup," in *Linear Accelerators*, edited by P. M. Lapostelle and A. L. Septier (North-Holland, Amsterdam, 1970), Chap. B.1.4, p. 173.
[3] V. K. Neil and R. K. Cooper, Part. Accel. 1, 111 (1970).
[4] V. K Neil, L. S. Hall, and R. K. Cooper, Part. Accel. 9, 213 (1979).
[5] A. W. Chao, B. Richter, and C. Y. Yao, Nucl. Instrum. Methods 178, 1 (1980).
[6] R. L. Gluckstern, R. K. Cooper, and P. J. Channell, Part. Accel. 16, 125 (1985).
[7] Y. Y. Lau, Phys. Rev. Lett. 63, 1141 (1989).
[8] S. Humphries, Jr., *Principles of Charged Particle Acceleration* (Wiley, New York, 1986).
[9] R. A. Bosch and R. M. Gilgenbach, Appl. Phys. Lett. 58, 699 (1991).
[10] P. R. Menge, R. A. Bosch, R. M. Gilgenbach, J. J. Choi, H. Ching, and T. A. Spencer, Proc. SPIE 1407, 578 (1991).
[11] R. M. Gilgenbach, P. R. Menge, R. A. Bosch, J. J. Choi, H. Ching, and T. A. Spencer, in *Proceedings of the 1991 IEEE Particle Accelerator Conference* (IEEE, New York, 1991).
[12] Y. Y. Lau, NRL Memo Report No. 6237, 1988.
[13] P. Allison, M. J. Burns, G. J. Caporaso, and A. G. Cole, in *Proceedings of the 1991 IEEE Particle Accelerator Conference* (IEEE, New York, 1991); also available as Los Alamos Report LA-UR-90-4224.
[14] Y. Y. Lau (private communication).
[15] Y. Y. Lau and D. G. Colombant, Appl. Phys. Lett. 55, 2673 (1989).
[16] C. L. Bohn and J. R. Delayen, Proc. SPIE 1407, 566 (1991).
[17] J. R. Delayen and C. L. Bohn, *Proceedings of the 1991 IEEE Particle Accelerator Conference* (IEEE, New York, 1991).
[18] K. A. Thompson and R. D. Ruth, Phys. Rev. D 41, 964 (1990).

Presented at SPIE's OE/LASE Conference, Los Angeles CA, January 1992

Beam Breakup Instability Experiments on Long-Pulse Electron-Beam Transport through RF Cavities

P.R. Menge, R.M. Gilgenbach, R.A. Bosch, H. Ching, T.A. Spencer, and M. Walter

Intense Energy Beam Interaction Laboratory, Department of Nuclear Engineering, Cooley Building, North Campus, The University of Michigan, Ann Arbor, MI 48109-2104

ABSTRACT

Experiments designed to investigate the beam breakup (BBU) instability have been performed using the long-pulse MELBA electron-beam generator (0.5 - 1.5 μs, 0.7 - 0.8 MV, I_{diode} = 1-15 kA, $I_{extracted}$ = 0.1-0.5 kA). The experiment consists of 10 identical pillbox cavities each containing a small microwave loop antenna designed to detect the TM_{110} beam breakup mode. For our cavity design the TM_{110} resonant frequency occurs at approximately 2.5 GHz. The cavities are connected by small diameter tubes which attenuate the RF cavity-to-cavity crosstalk. The MELBA diode and subsequent cavity system are immersed in a solenoidal magnetic field (0.8 - 3 kG). Microwaves of 2.5 GHz (1 - 4 kW), whose pulselength exceeds the beam pulse, can be injected into the initial cavity in order the prime the BBU instability. BBU instability growth is measured through the growth of 2.5 GHz RF between the first (or second) and tenth cavities. The BBU growth is compared with predictions made by beam-cavity coupled-mode theory.

1. INTRODUCTION

A persistent problem plaguing high-brightness, long pulse charged particle accelerators is the beam breakup (BBU) instability[1-7]. Continuing experiments at the University of Michigan have been designed to investigate the BBU instability[8-9] with particular emphasis on characterizing its scaling laws and discovering suppression techniques. The experiment consists of ten nearly identical pillbox cavities through which a coasting electron beam is propagated. Each cavity contains a small microwave loop antenna designed to detect the non-axisymmetric TM_{110} mode. It is the asymmetry of this mode that produces transverse deflections in the beam[7]. Furthermore, the transverse e-beam deflections increase the strength of the TM_{110} mode. Thus, an unstable beam-cavity coupling arises (called BBU) which can cause numerous effects ranging from emittance degradation to loss of current[1,10]. By observing the growth of microwaves which correspond to the TM_{110} mode frequency (2.5 GHz), the growth rate for the BBU can be measured.

2. EXPERIMENTAL CONFIGURATION

The electron beam accelerator used in this research is the Michigan Electron Long Beam Accelerator (MELBA). The MELBA diode operates with the following parameters: voltage ≈ -0.7 to -0.8 MV, diode current = 1 - 10 kA, and pulselength = 0.3 - 5 μs, with flattop voltage provided by an Abramyan type compensation stage over 1.5 μs.

The experimental configuration is shown in Figure 1. The electron beam is generated from an explosive emission velvet cathode. This cathode consists of a glyptal coated

hemispherical-end cathode stalk with a velvet emitting button attached to the end of the cathode stalk. This cathode is advantageous for its slow diode closure, limited edge emission, and relatively long glyptal life[11]. The anode is a graphite plate (1/8 " thick) located 10.8 cm from the end of the cathode. A circular aperture with a diameter of 2 cm is centered on the anode plate to extract 40-300 A into the transport chamber.

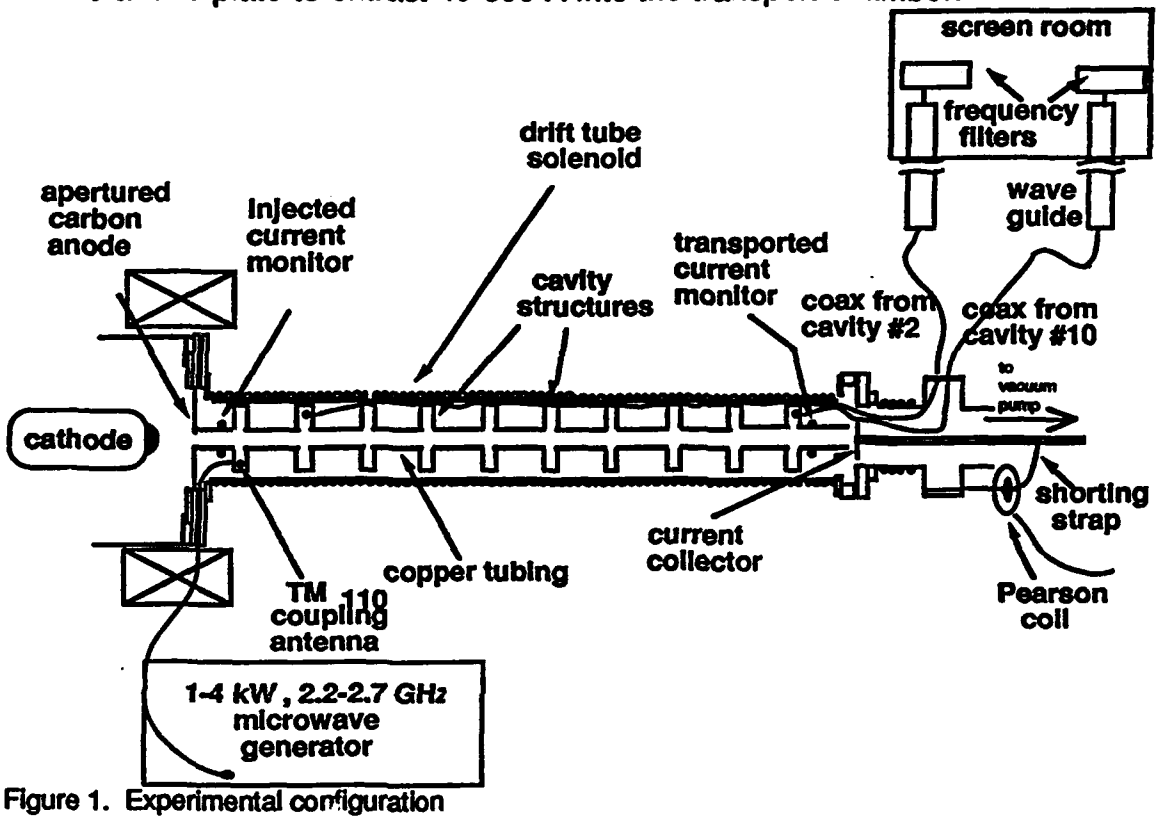

Figure 1. Experimental configuration

The diode chamber is immersed in a solenoidal magnetic field that can be varied from 0.5 - 1.2 kG. The transport chamber is composed of a 1 m long drift tube surrounded by solenoid coils pulsed independently from the diode. The current to the solenoid is provided by a 2-stage double-polarity electrolytic capacitor bank that produces a magnetic field up to 3.5 kG. Since the diode coils and the drift tube solenoid overlap, the superposition of the solenoidal fields causes a total B-field profile that is not quite uniform in the experimental chamber. The profile is higher on the upstream end before tapering to a flattop about halfway down the drift tube.

Within the drift tube are ten brass pillbox resonant cavities separated by smaller diameter copper tubes. Each cavity has a radius of 6.9 cm and a length of 2.0 cm. Within each cavity is a small loop antenna sensitive to the TM_{110} cavity mode. The length of the separation tubes is 6.5 cm, giving an intercavity distance of 8.5 cm. The diameter of the tubes is 3.8 cm, which is below the TM_{010} cutoff diameter, and thus serves to isolate each cavity from RF crosstalk. The measured attenuation of the 2.5 GHz, TM_{110} mode microwaves is 26 dB from cavity to adjacent cavity.

The first cavity (closest to the anode) has its TM_{110} mode primed externally by an Epsco (model PG5KB) microwave pulse generator. The priming microwave pulse is

generally 3 μs long and begins before the e-beam is present. The power of the injected microwaves is generally 1 kW.

In the second cavity the e-beam-induced RF is measured via the loop antenna. The microwaves are propagated out of the experimental chamber through RG/.405 U semi-rigid transmission cable to a vacuum feedthrough to RG/8 cable to an S-band waveguide. The waveguide runs to a screened room where the signal is attenuated and filtered for frequency information. Part of the microwave signal is diverted into a filter that passes 2.5 GHz ± 11 MHz. This frequency, as noted above, corresponds to the TM_{110} beam breakup frequency.

The RF in the tenth (last) cavity is measured in the same way with its own set of cables and waveguide. The growth of the BBU instability is determined by the decibels of growth in 2.5 GHz microwave power between the second and tenth cavities.

The e-beam current is measured before entering the first cavity and after exiting the last cavity using calibrated Rogowski coils.

3. EXPERIMENTAL DATA and RESULTS

Two experimental cases have been investigated. The first case employed cavities with a relatively high Q and moderate frequency spread. The second case used cavities with a low Q and small frequency spread. Table 1 lists the TM_{110} resonance frequencies and their corresponding Q's.

Table 1

		Case 1		Case 2	
	Cavity #	TM_{110} freq. (GHz)	Q	TM_{110} freq. (GHz)	Q
(Driven)	1	2.5190	660	2.5070	230
(Probed)	2	2.5200	1090	2.5070	290
	3	2.5200	1420	2.5060	215
	4	2.5201	1800	2.5066	220
	5	2.5265	530	2.5071	280
	6	2.5270	680	2.5076	230
	7	2.5230	1160	2.5082	160
	8	2.5240	920	2.5082	185
	9	2.5248	680	2.5085	180
(Probed)	10	2.5250	1010	2.5086	170

For Case 1 the average TM_{110} resonance frequency is 2.5230 GHz ± 8.0 MHz, and the average Q is 1000 ± 390. For Case 2 the average resonance frequency is 2.5075 GHz ± 2.6 MHz, and the average Q is 215 ± 45.

3.1. High Q Results

A typical set of data signals for the high Q case (Case 1) is shown in figure 2. The top trace (a) is the MELBA diode voltage with the flattop corresponding to -750 kV. The next trace

(b) shows the injected current (i.e. the amount of current entering the first cavity) with a maximum of 200 A. The center signal (c) is the transported current (i.e. the amount of current exiting the last cavity) with a maximum of about 42 A. The next signal (d) is the 2.5 GHz RF power in the second cavity; this signal has been attenuated by 12 dB. The bottom trace (e) is the 2.5 GHz RF power in the tenth cavity; this signal has been attenuated by 32 dB. Allowing for the difference in signal amplitude and sensitivity of the microwave detectors, the growth of the 2.5 GHz microwaves is computed to be 26 dB, or 3.25 dB per cavity. This data was taken at a solenoidal magnetic field of 1.1 kG.

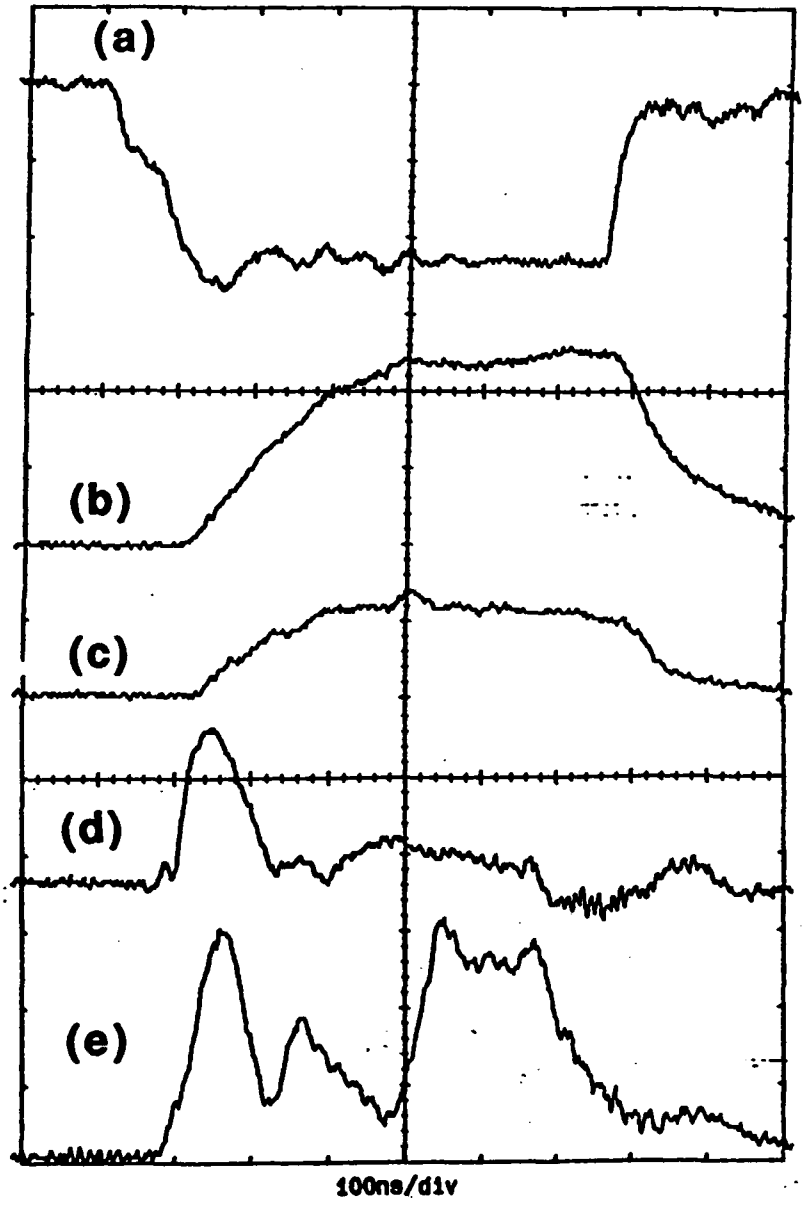

Figure 2. Sample data taken from two similar MELBA shots utilizing Case 1 cavities: a) Diode voltage (310 kV/div), flattop is -750 kV. b) Injected current (92 A/div), maximum is 230 A. c) Transported current (41 A/div), flattop is 46 A. d) 2nd cavity RF (100 mV/div), signal attenuated by 12 dB. e) 10th cavity RF (100 mV/div), signal is attenuated by 32 dB. Time scale is 100 ns/div. Solenoidal magnetic field is 1.1 kG.

The expected amount of BBU growth can be obtained from a discrete cavity theory[12] applicable to solenoidal focusing. The appropriate dispersion relation is:

$$k(\omega) = \frac{\omega}{v} \pm \frac{\omega_c}{2v} - \frac{1}{L}\,\mathrm{Arccos}\left(\cos\frac{L\omega_c}{2v} + \frac{\Gamma L}{\omega_c v}\sin\frac{L\omega_c}{2v}\right)$$

where, k is the wavenumber, ω is the angular frequency of the BBU wave, v is the e-beam velocity, ω_c is the betatron angular frequency, L is the distance between adjacent cavity centers,

$$\Gamma = \frac{2\omega_0{}^4\varepsilon}{-\omega^2+\omega_0{}^2+\frac{i\omega\omega_0}{Q}},$$

ω_0 is the angular frequency of the TM_{110} mode, Q is the quality factor of the cavities, and ε is the dimensionless coupling factor[13].

Using the data from figure 2, the theoretical amplitude of BBU growth is 29 dB. This agrees well with the (26 dB) experimental growth in the 2.5 GHz microwaves. Figure 3 shows the theoretical and experimental values of BBU growth for various current amplitudes. At the higher current values the difference between theory and experiment becomes more

pronounced. This could be due to e-beam detuning of the cavities' TM_{110} resonance frequencies. At about 120 A the e-beam will upshift the resonant frequency[14] by 0.05 %. This is enough to shift the frequency out of the Q curve if Q = 1000. Thus, the theoretical BBU growth would be expected to be greater than experiment since the theory assumes less detuning. Figure 4 illustrates the experimental growth rates plotted versus the current to magnetic field ratio, I/B. Since the experiment is operated in the "weak focusing" growth regime[7], the BBU growth rate is expected to be approximately linear in I/B. The divergence of the two plots suggests the e-beam detuning of the cavities.

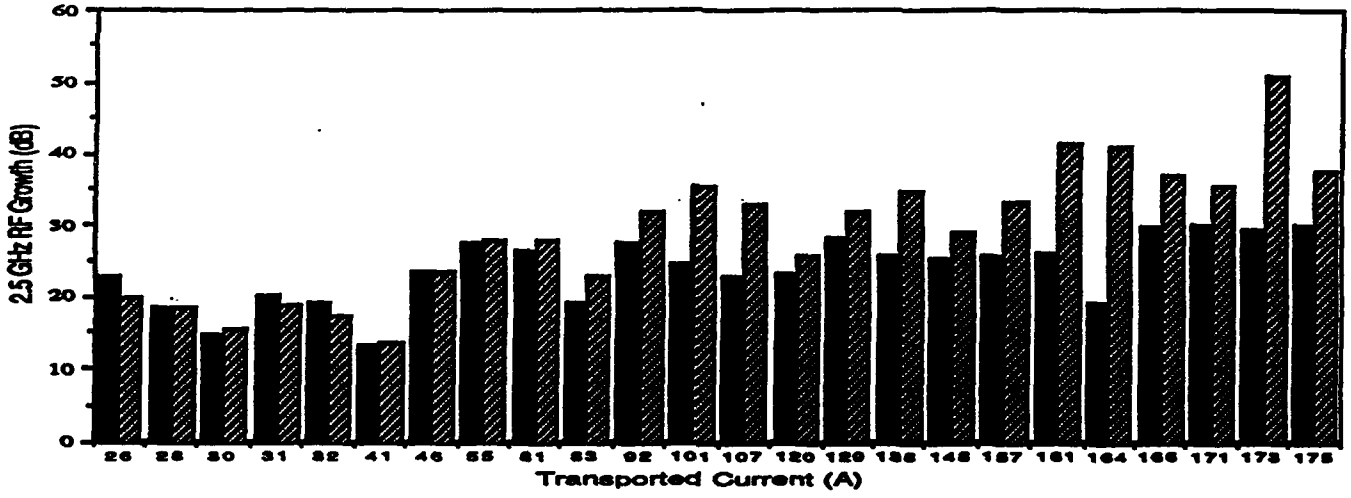

Figure 3. Column graph comparing the experimental (solid bars) growth of the BBU instability to the theoretical (cross-hatched bars) growth as the current is increased. The growth does not necessarily increase with the current because the magnetic field is not constant as current is changed.

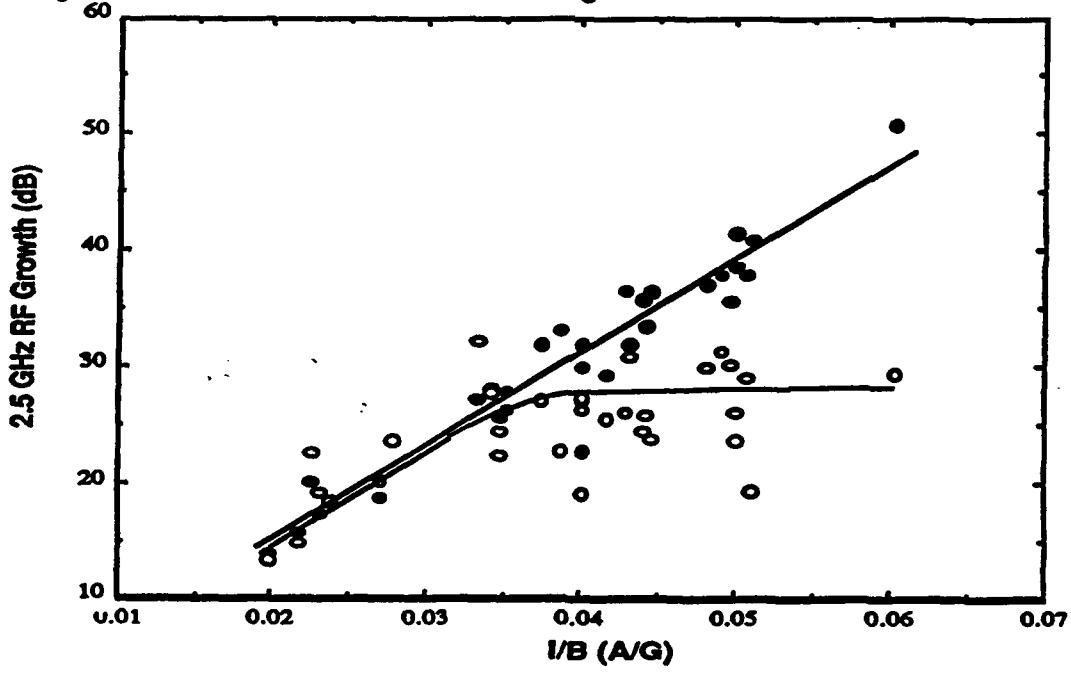

Figure 4. Graph showing the dependence of experimental (open circles) and theoretical (closed circles) growth on the ratio of current to magnetic field, I/B. Solid lines are a guide for the eye.

In order to gain insight into the detuning phenomenon, experiments were carried out in which the system was purposely detuned by priming the first cavity at frequencies other than its TM_{110} resonant frequency. The current was maintained at a low level (≈40 A) which avoids current detuning. Significant reduction of the 2.5 GHz microwaves occurred when the priming RF was detuned only slightly (≈ 0.2 %). Figure 5 shows that the growth of BBU RF has a width comparable to the Q curve of the TM_{110} cavity mode. These data prove that the TM_{110} BBU mode is responsible for the observed microwave amplification.

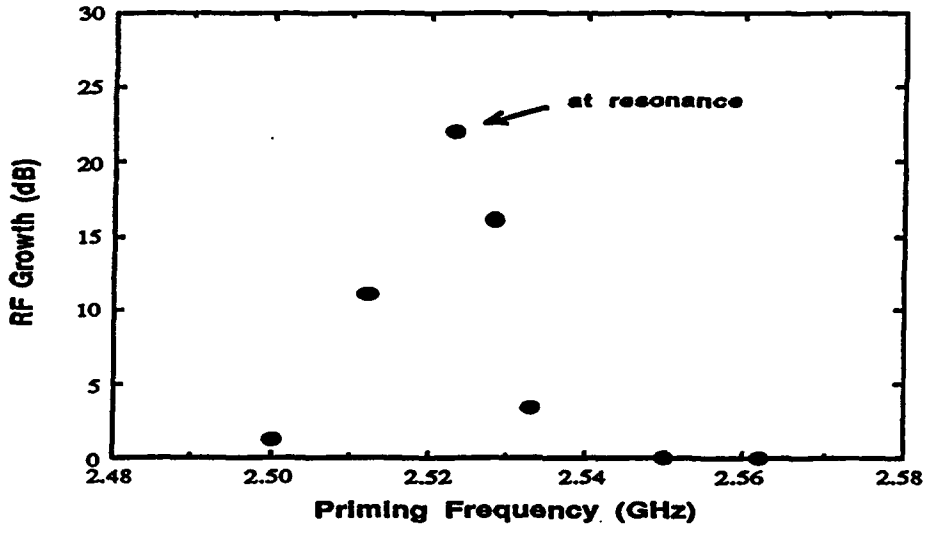

Figure 5. Plot showing the effect of varying the priming frequency of the initial cavity. All points were taken at nearly identical magnetic fields (1.1 kG) and currents (40 A). Resonant point is the average of 3 shots.

3.2. Low Q Results

Since the Case 1 cavities have a relatively large average Q and resonant frequency spread, the amount of BBU instability growth is limited by stagger detuning[15], because the Q curves of all the cavities do not overlap. This motivated a change to cavities with a lower average Q so that the system is less sensitive to spread in the TM_{110} mode frequency. Since a low Q lessens the effect of this stagger detuning, greater instability growth can be expected. For the Case 2 cavities the average Q has been lowered by a factor of five, and the spread in TM_{110} resonant frequencies has been reduced by a factor of three.

Figure 6 shows a sample data set using the Case 2 cavities. The uppermost trace (a) is the MELBA diode voltage with the flattop corresponding to -750 kV. The next trace (b) shows the injected current with a maximum of 200 A. The center signal (c) is the transported current with a maximum of about 165 A. The next signal (d) is the 2.5 GHz RF power in the second cavity; this signal has been attenuated by 6 dB. The lowest trace (e) is the 2.5 GHz RF power in the tenth cavity; this signal has been attenuated by 35 dB. Allowing for the difference in signal amplitude and sensitivity of the microwave detectors, the growth of the 2.5 GHz microwaves is computed to be 38 dB, or 4.8 dB per cavity. These data were taken at a

solenoidal magnetic field of 2.1 kG. Using these data in the previous theory, the predicted amount of BBU instability growth is 44 dB.

Figure 7 is a plot of 2.5 GHz microwave growth for the Case 2 cavities versus the ratio of e-beam current to magnetic field, I/B. The experimental growth data maintains a relatively linear shape in contrast to the Case 1 data in figure 4. This suggests that there is less cavity detuning from the high current beam in the low Q case.

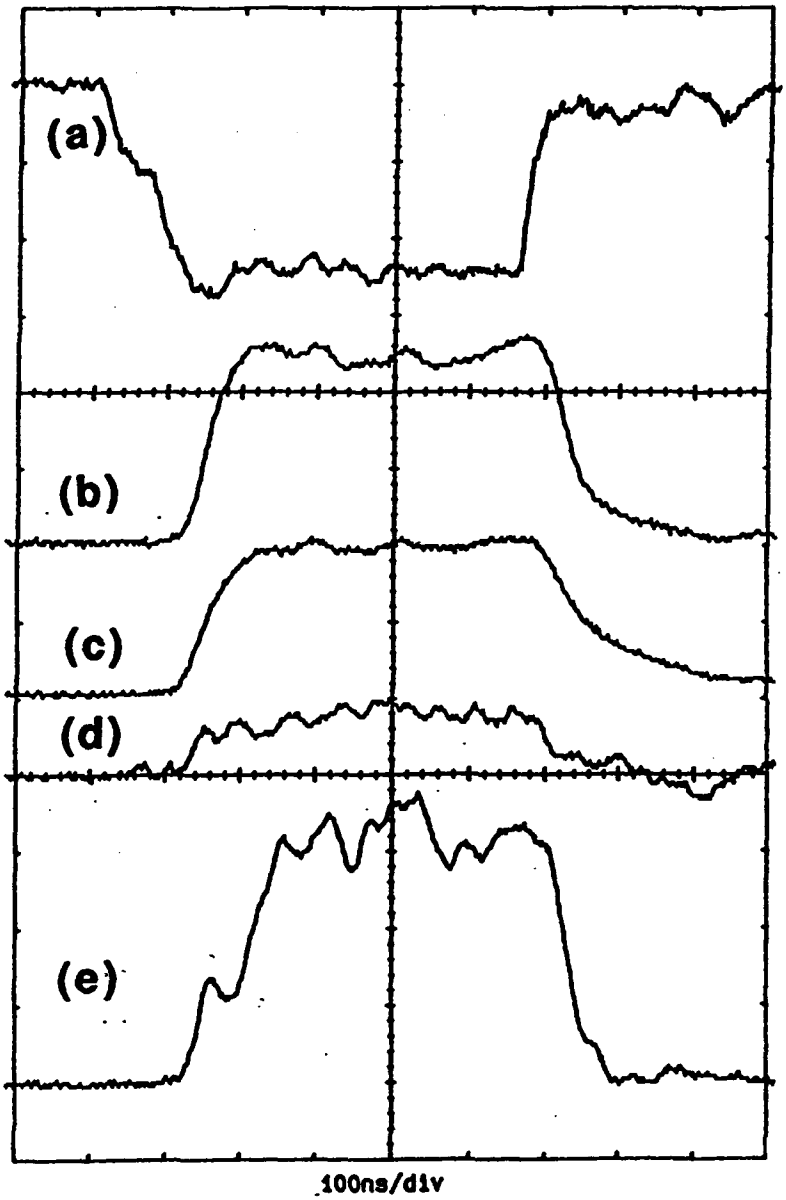

Figure 6. Sample data taken from two similar MELBA shots utilizing Case 2 cavities. a) Diode voltage (310 kV/div), flattop is -750 kV. b) Injected current (92 A/div), maximum is 250 A. c) Transported current (92 A/div), flattop is 200 A. d) 2nd cavity RF (100 mV/div), signal attenuated by 6 dB. e) 10th cavity RF (100 mV/div), signal is attenuated by 35 dB. Time scale is 100 ns/div. Solenoidal magnetic field is 2.1 kG.

4. CONCLUSIONS

The beam breakup experiments at the University of Michigan have achieved the following results:

1) The BBU instability has been successfully excited by RF priming of the initial cavity.
2) Theoretical BBU growth accurately describes TM_{110} microwave growth for low current e-beams (<100 A) when cavity Q's are about 1000.
3) Divergence of theoretical and experimental BBU growth rates at high currents (>100 A) could be due to detuning of the TM_{110} mode from the frequency upshift caused by the e-beam.
4) Strong BBU growth (2.5-4.8 dB/cavity) is observed only when the initial cavity is primed at the precise TM_{110} mode resonant frequency (<<1% detuning).
5) High current e-beam detuning can possibly be avoided by lowering cavity Q's (from 1000 to 200).
6) Reducing the spread in the TM_{110} mode resonant frequency increases the amount of BBU growth per cavity

5. ACKNOWLEDGEMENTS

This research is sponsored by SDIO through an ONR grant. We thank Dr. Y.Y. Lau for valuable discussions.

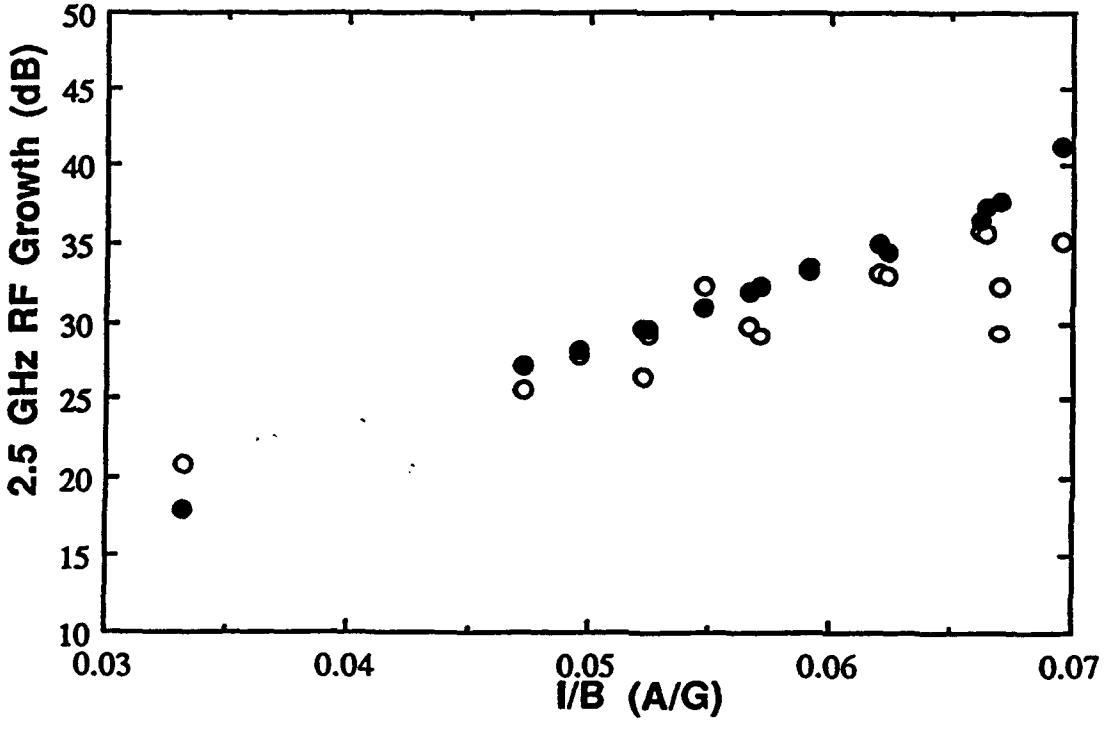

Figure 7. Graph showing the dependence of experimental (open circles) and theoretical (closed circles) growth on the ratio of current to magnetic field, I/B.

6. REFERENCES

1. W.K.H. Panofsky and M. Bander, Rev. Sci. Instrum. **39**, 206 (1968).
2. R. Helm and G. Loew, Beam Breakup, Chapter B.1.4 in *Linear Accelerators*, P.M. Lapostelle and A.L. Septier, Editors, p. 173 (North Holland Publishing Co., Amsterdam, 1970).
3. V.K. Neil and R.K. Cooper, Part. Accel. **1**, 111 (1970).
4. V.K. Neil, L.S. Hall, and R.K. Cooper, Part. Accel. **9**, 213 (1979).
5. A.W. Chao, B. Richter, and C.Y. Yao, Nucl. Instrum. Methods **178**, 1 (1980).
6. R.L. Gluckstern, R.K. Cooper, and P.J. Channell, Part. Accel. **16**, 125 (1985).
7. Y.Y. Lau, Phys. Rev. Lett. **63**, 1141 (1989).
8. P.R. Menge, R.A. Bosch, R.M. Gilgenbach, J.J. Choi, H. Ching, and T.A. Spencer, in *Intense Microwaves and Particle Beams II*, H.E. Brandt, Editor, Proc. SPIE 1407, p. 578 (SPIE, Bellingham, WA, 1991).
9. R.M. Gilgenbach, P.R. Menge, R.A. Bosch, J.J. Choi, H. Ching, and T.A. Spencer, in *Proceedings of the 1991 IEEE Particle Accelerator Conference*, (IEEE, New York, NY, 1991).
10. Y.Y. Lau, NRL Memo Report No. 6237, 1988.
11. T.A. Spencer, Doctoral Thesis, Univ. of Mich., Dept. of Nuc. Eng., 1991
12. R.A. Bosch, P.R. Menge, and R.M. Gilgenbach to be published in J. Appl. Phys., April 1, 1992.
13. The epsilon factor for the TM_{110} mode is $\varepsilon \approx 0.422 \frac{\ell}{L} \frac{I\,(kA)}{17} \frac{\beta}{\gamma}$, where ℓ is the cavity length, L is the cavity spacing, I is the beam current, and β and γ are the usual relativistic velocity and mass factors. See references 7, 10 , and 15 for further explanation.
14. R.E. Shefer and G. Bekefi, Int. J. Electronic **51**(4), 569 (1981)
15. D.G. Colombant and Y.Y. Lau, Appl. Phys. Lett. **55**(1), 27 (1989)